

Role of bias and tunneling asymmetries in nonlinear Fermi-liquid transport through an $SU(N)$ quantum dot

Kazuhiko Tsutsumi,^{1,2} Yoshimichi Teratani,^{1,2} Kaiji Motoyama,¹ Rui Sakano,³ and Akira Oguri^{1,2}

¹*Department of Physics, Osaka City University, Sumiyoshi-ku, Osaka 558-8585, Japan*

²*NITEP, Osaka Metropolitan University, Sumiyoshi-ku, Osaka 558-8585, Japan*

³*Department of Physics, Keio University, 3-14-1 Hiyoshi, Kohoku-ku, Yokohama, Kanagawa 223-8522, Japan*

(Dated: May 3, 2023)

We study how bias and tunneling asymmetries affect nonlinear current through a quantum dot with N discrete levels in the Fermi liquid regime, using an exact low-energy expansion of the current derived up to terms of order V^3 with respect to the bias voltage. The expansion coefficients are described in terms of the phase shift, the linear susceptibilities, and the three-body correlation functions, defined with respect to the equilibrium ground state of the Anderson impurity model. In particular, the three-body correlations play an essential role in the order V^3 term, and their coupling to the nonlinear current depends crucially on the bias and tunnel asymmetries. The number of independent components of the three-body correlation functions increases with N the internal degrees of the quantum dots, and it gives a variety in the low-energy transport. We calculate the correlation functions over a wide range of electron fillings of the Anderson impurity model with the $SU(N)$ internal symmetry, using the numerical renormalization group. We find that the order V^3 nonlinear current through the $SU(N)$ Kondo state, which occurs at electron fillings of 1 and $N - 1$ for strong Coulomb interactions, significantly varies with the three-body contributions as tunnel asymmetries increase. Furthermore, in the valence fluctuation regime toward the empty or fully occupied impurity state, a sharp peak emerges in the coefficient of V^3 current in the case at which bias and tunneling asymmetries cooperatively enhance the charge transfer from one of the electrodes.

I. INTRODUCTION

The ground state and low-lying excited states of quantum-impurity systems [1, 2] such as dilute magnetic alloys and quantum dots can be described as a local Fermi liquid [3–7], in which localized electrons with discrete energies are strongly coupled to conduction electrons in host metals or electrodes. These low-energy states continuously evolve as the occupation number of the discretized states varies, and various interesting phenomena such as the Kondo effects and the valence fluctuations occur, depending on electron fillings and the configurations [8–10].

After early observations of the Kondo effect in quantum dots [11–17], universal Fermi-liquid behaviors were explored through highly sensitive measurements [18–23] and precise calculations [24–27]. Furthermore, various kinds of internal degrees of freedom bring an interesting variety to the Kondo effects in quantum dots, such as the one with the $SU(4)$ symmetry that can be realized in multi-orbital dots and in carbon-nanotube (CNT) dots [28–44]. External magnetic fields also induce interesting crossover phenomena, such as the one between the $SU(4)$ and $SU(2)$ Kondo states observed in a CNT quantum dot [45–48].

Recent development in the Fermi-liquid theory also reveals that the three-body correlations of electrons passing through the quantum dot play an essential role in the next-leading order terms of the transport coefficients [49–53] when the system does not have both electron-hole and time-reversal symmetries. This is because, in addition

to the well-studied damping of order ω^2 , T^2 , and $(eV)^2$, quasiparticles of the local Fermi liquid capture the energy shift of the same quadratic order which is induced by the three-body correlations, at low but finite frequencies ω , temperatures T , and bias voltages eV . The three-body contributions have also been confirmed experimentally in magnetoconductance measurements very recently [54].

Here we focus on the effects of bias and tunneling asymmetries on the nonlinear current I at low energies. Specifically, we examine the bias asymmetry that can be described by the parameter $(\mu_L + \mu_R)/2 - E_F$, with μ_L and μ_R the chemical potentials of the source (L) and drain (R) electrodes, applied such that $eV \equiv \mu_L - \mu_R$, and E_F the Fermi level at thermal equilibrium $eV = 0$. The other one, tunneling asymmetry, occurs through the difference between the tunnel couplings Γ_L and Γ_R for the source and drain electrodes, respectively. In the previous paper, we demonstrated how these asymmetries affect the transport through a quantum dot described by a spin-1/2 Anderson impurity model with no orbital degrees of freedom [55], and showed that the three-body correlations give significant contributions to the order $(eV)^3$ nonlinear current in the valence fluctuation regime, using the numerical renormalization group (NRG) approach.

The purpose of this paper is to clarify how the conjunction of these asymmetries and the internal degrees of freedom, which increases the independent components of the three-body correlation functions, affects low-energy transport in the Fermi-liquid regime. The low-bias expansion of the conductance up to terms order $(eV)^2$ can be described by the Fermi-liquid theory with the three-

body correlations, which at zero temperature $T = 0$ takes the following form for a quantum dot with N discrete levels which include the spin components,

$$\frac{dI}{dV} = g_0 \sum_{\sigma=1}^N \left[\sin^2 \delta_{\sigma} + c_{V,\sigma}^{(2)} eV - c_{V,\sigma}^{(3)} (eV)^2 + \dots \right]. \quad (1.1)$$

Here, $g_0 = (e^2/h) 4\Gamma_L \Gamma_R / (\Gamma_L + \Gamma_R)^2$, which depends on tunneling asymmetries. We present the exact formulas for the coefficients $c_{V,\sigma}^{(2)}$ and $c_{V,\sigma}^{(3)}$ of the multilevel Anderson impurity model which are applicable to arbitrary impurity electron fillings and arbitrary level structures $\epsilon_{d\sigma}$. These coefficients are determined by the phase shift δ_{σ} and the other renormalized parameters, including the three-body correlation functions, and depend crucially on the bias and tunneling asymmetries. We show that, for $N \geq 3$, the three-body correlations between electrons in three different levels also couple to order $(eV)^3$ nonlinear current as well as the other components when there are some extents of bias and/or tunneling asymmetries. Our formula includes the previous results of the other group as some special limiting cases: $c_{V,\sigma}^{(2)}$ derived by Aligia for the Anderson model [56, 57], and $c_{V,\sigma}^{(3)}$ derived by Mora *et al.* for the $SU(N)$ Kondo model [40].

We also calculate $c_{V,\sigma}^{(2)}$ and $c_{V,\sigma}^{(3)}$ for the $SU(N)$ symmetric quantum dots with $N = 4$ and 6 , using the NRG in a wide range of electron fillings, varying the parameter corresponding to the gate voltage. There emerge $(N - 1)$ different Kondo states in the $SU(N)$ symmetric case, which can be classified according to the occupation number $\langle n_d \rangle = 1, 2, \dots, N - 1$. We find that large Coulomb interaction suppresses charge fluctuations throughout the region of $1 \lesssim \langle n_d \rangle \lesssim N - 1$, and it makes the coefficients $c_{V,\sigma}^{(2)}$ and $c_{V,\sigma}^{(3)}$ less sensitive to the bias asymmetry, whereas the tunneling asymmetry affects these coefficients. In particular, in the $SU(N)$ Kondo states at electron fillings of $\langle n_d \rangle \simeq 1$ and $N - 1$ for $N \geq 3$, the three-body contributions become sensitive to tunnel asymmetries, and it significantly varies the behavior of the order $(eV)^3$ nonlinear current.

In contrast, in the valence fluctuation regime toward the empty or fully occupied impurity state, i.e., at $0 \lesssim \langle n_d \rangle \lesssim 1$ or $N - 1 \lesssim \langle n_d \rangle \lesssim N$, both the bias and tunneling asymmetries affect the nonlinear transport. We find that, in these regions, a sharp peak emerges in the coefficient $c_{V,\sigma}^{(3)}$, in the case at which the bias and tunneling asymmetries cooperatively enhance the charge transfer from one of the electrodes.

This paper is organized as follows. In Sec. II, we describe an outline of the microscopic Fermi-liquid theory for the multilevel Anderson model, and derive the low-energy asymptotic form of the differential conductance. Section III shows the NRG results of quasiparticle parameters for $SU(4)$ and $SU(6)$ quantum dots. In Secs. IV and V, we show the NRG results for the coefficients $c_{V,\sigma}^{(2)}$

and $c_{V,\sigma}^{(3)}$, respectively. Summary is given in Sec. VI.

II. FORMULATION

We consider a quantum dot with N -level coupled to two noninteracting leads by using the Anderson Hamiltonian:

$$H = H_d + H_c + H_T \quad (2.1)$$

$$H_d = \sum_{\sigma=1}^N \epsilon_{d\sigma} n_{d\sigma} + \frac{U}{2} \sum_{\sigma \neq \sigma'} n_{d\sigma} n_{d\sigma'}, \quad (2.2)$$

$$H_c = \sum_{\nu=L,R} \sum_{\sigma=1}^N \int_{-D}^D d\epsilon \epsilon c_{\epsilon\nu\sigma}^{\dagger} c_{\epsilon\nu\sigma}, \quad (2.3)$$

$$H_T = \sum_{\nu=L,R} \sum_{\sigma=1}^N v_{\nu} (\psi_{\nu,\sigma}^{\dagger} d_{\sigma} + d_{\sigma}^{\dagger} \psi_{\nu,\sigma}), \quad (2.4)$$

$$\psi_{\nu,\sigma} \equiv \int_{-D}^D d\epsilon \sqrt{\rho_c} c_{\epsilon\nu\sigma}. \quad (2.5)$$

Here, d_{σ}^{\dagger} for $\sigma = 1, 2, \dots, N$ creates an impurity electron with energy $\epsilon_{d\sigma}$, $n_{d\sigma} \equiv d_{\sigma}^{\dagger} d_{\sigma}$, and U is the Coulomb interaction between electrons in the quantum dot. $c_{\epsilon\nu\sigma}^{\dagger}$ creates an electron with energy ϵ in the lead on the left or right ($\nu = L, R$), and it is normalized as $\{c_{\epsilon\nu\sigma}, c_{\epsilon'\nu'\sigma'}^{\dagger}\} = \delta(\epsilon - \epsilon') \delta_{\nu\nu'} \delta_{\sigma\sigma'}$. The linear combination of the conduction electron $\psi_{\nu,\sigma}$ couples to the dot via the tunneling matrix element v_{ν} . It determines the resonance width of the impurity level $\Delta = \Gamma_L + \Gamma_R$, with $\Gamma_{\nu} \equiv \pi \rho_c v_{\nu}^2$ the tunnel energy scale due to the lead ν , and $\rho_c = 1/(2D)$ the density of state of the conduction band with a half-width D . We set $k_B = 1$ throughout this paper, and consider the parameter region where the half bandwidth D is much greater than the other energy scales, $D \gg \max(U, \Delta, |\epsilon_{d\sigma}|, T, |eV|)$.

A. Fermi-liquid parameters

We describe here the definition of the correlation functions that play an essential role in the microscopic Fermi-liquid theory.

The occupation number and the linear susceptibilities of the impurity level can be derived from the free energy:

$$\langle n_{d\sigma} \rangle = \frac{\partial \Omega}{\partial \epsilon_{d\sigma}}, \quad \Omega \equiv -T \log [\text{Tr} e^{-\beta H}], \quad (2.6)$$

$$\chi_{\sigma\sigma'} \equiv -\frac{\partial^2 \Omega}{\partial \epsilon_{d\sigma} \partial \epsilon_{d\sigma'}} = \int_0^{\beta} d\tau \langle \delta n_{d\sigma}(\tau) \delta n_{d\sigma'} \rangle, \quad (2.7)$$

where $\delta n_{d\sigma} = n_{d\sigma} - \langle n_{d\sigma} \rangle$, and $\langle \dots \rangle$ represents an equilibrium average, with $\beta = 1/T$ the inverse temperature.

In addition to linear susceptibilities, the nonlinear ones $\chi_{\sigma_1\sigma_2\sigma_3}^{[3]}$ also play an important role away from half filling:

$$\begin{aligned} \chi_{\sigma_1\sigma_2\sigma_3}^{[3]} &\equiv -\frac{\partial^3\Omega}{\partial\epsilon_{d\sigma_1}\partial\epsilon_{d\sigma_2}\partial\epsilon_{d\sigma_3}} = \frac{\partial\chi_{\sigma_1\sigma_2}}{\partial\epsilon_{d\sigma_3}} \\ &= -\int_0^\beta d\tau_1 \int_0^\beta d\tau_2 \langle T_\tau \delta n_{d\sigma_1}(\tau_1) \delta n_{d\sigma_2}(\tau_2) \delta n_{d\sigma_3} \rangle. \end{aligned} \quad (2.8)$$

Here, T_τ is the imaginary-time ordering operator. This correlation function has the permutation symmetry: $\chi_{\sigma_1\sigma_2\sigma_3}^{[3]} = \chi_{\sigma_2\sigma_1\sigma_3}^{[3]} = \chi_{\sigma_3\sigma_2\sigma_1}^{[3]} = \chi_{\sigma_1\sigma_3\sigma_2}^{[3]} = \dots$. We will use hereafter the ground state values for $\langle n_{d\sigma} \rangle$, $\chi_{\sigma\sigma'}$ and $\chi_{\sigma_1\sigma_2\sigma_3}^{[3]}$, and thus the occupation number can be deduced from the phase shift δ_σ through the Friedel sum rule: $\langle n_{d\sigma} \rangle \xrightarrow{T \rightarrow 0} \delta_\sigma/\pi$ [6].

The retarded Green's function also plays a central role in the microscopic description of the Fermi-liquid transport:

$$G_\sigma^r(\omega) = -i \int_0^\infty dt e^{i(\omega+i0^+)t} \left\langle \left\{ d_\sigma(t), d_\sigma^\dagger \right\} \right\rangle_{eV}, \quad (2.9)$$

$$A_\sigma(\omega) \equiv -\frac{1}{\pi} \text{Im} G_\sigma^r(\omega). \quad (2.10)$$

represents a nonequilibrium steady-state average taken with the statistical density matrix, which is constructed at finite bias voltages eV and temperatures T , using the Keldysh formalism [58, 59].

The phase shift δ_σ is related to the value of the Green's function at the equilibrium ground state $T = eV = 0$ as $G_\sigma^r(0) = -|G_\sigma^r(0)| e^{i\delta_\sigma}$. It also determines the behavior of the equilibrium spectral function $\rho_{d\sigma}(\omega) \equiv A_\sigma(\omega)|_{T=eV=0}$ in the low-frequency limit. At the Fermi level $\omega = 0$, it takes the form

$$\rho_{d\sigma} \equiv \rho_{d\sigma}(0) = \frac{\sin^2 \delta_\sigma}{\pi \Delta}. \quad (2.11)$$

Furthermore, the first derivative of $\rho_{d\sigma}(\omega)$ is related to the diagonal susceptibility $\chi_{\sigma\sigma}$, as

$$\rho'_{d\sigma} \equiv \left. \frac{\partial \rho_{d\sigma}(\omega)}{\partial \omega} \right|_{\omega=0} = \frac{\chi_{\sigma\sigma}}{\Delta} \sin 2\delta_\sigma. \quad (2.12)$$

This is a result of a series of exact Fermi-liquid relations, obtained by Yamada-Yosida [see Appendix A].

B. Low-energy expansion of nonlinear current

Nonlinear current through quantum dots can be calculated using a Landauer-type formula [58, 59]:

$$\begin{aligned} I &= \frac{e}{h} \frac{4\Gamma_L\Gamma_R}{(\Gamma_L + \Gamma_R)^2} \\ &\times \sum_{\sigma=1}^N \int_{-\infty}^{\infty} d\omega [f_L(\omega) - f_R(\omega)] \pi \Delta A_\sigma(\omega). \end{aligned} \quad (2.13)$$

Here, $f_\nu(\omega) = [e^{\beta(\omega - \mu_\nu)} + 1]^{-1}$ is the Fermi distribution function for the conduction band on $\nu = L, R$. The chemical potential of the left and right leads are driven from the Fermi energy at equilibrium $E_F = 0$ by the gate voltage: $\mu_L = \alpha_L eV$ and $\mu_R = -\alpha_R eV$, with α_L and α_R the parameters which satisfy $\alpha_L + \alpha_R = 1$, i.e., $\mu_L - \mu_R \equiv eV$. Asymmetries in tunnel couplings and that in bias voltages can be described, respectively, by the following parameters,

$$\gamma_{\text{dif}} \equiv \frac{\Gamma_L - \Gamma_R}{\Gamma_L + \Gamma_R}, \quad (2.14)$$

$$\alpha_{\text{dif}} \equiv \frac{\mu_L + \mu_R}{\mu_L - \mu_R} = \alpha_L - \alpha_R. \quad (2.15)$$

In this work, we have derived the explicit expressions of the coefficients $c_{V,\sigma}^{(2)}$ and $c_{V,\sigma}^{(3)}$ for the first two nonlinear-response terms of dI/dV in Eq. (1.1), using the exact low-energy asymptotic form of the spectral function $A_\sigma(\omega)$ of quantum dots embedded in asymmetric junctions obtained up to terms of order ω^2 , $(eV)^2$, and T^2 . The derivation is given in Appendix B. Specifically, we will use Eqs. (B5) and (B6) to clarify the roles of the tunnel and bias asymmetries, which enter through the parameters γ_{dif} and α_{dif} , in the nonlinear Fermi-liquid transport.

1. dI/dV of an $SU(N)$ dot with tunnel and bias asymmetries

In this paper, we consider the $SU(N)$ symmetric case, at which the impurity level has the N -fold degeneracy: $\epsilon_{d\sigma} \equiv \epsilon_d$ for $\sigma = 1, 2, \dots, N$. For convenience, we use a shifted impurity energy level, defined by $\xi_d \equiv \epsilon_d + (N-1)U/2$ in the following. Note that the system additionally has an electron-hole symmetry at $\xi_d = 0$.

The linear susceptibilities have two independent components in the $SU(N)$ symmetric case, i.e., the diagonal component $\chi_{\sigma\sigma}$ and the off-diagonal one $\chi_{\sigma\sigma'}$ for $\sigma \neq \sigma'$. These two parameters determine the essential properties of quasiparticles:

$$T^* \equiv \frac{1}{4\chi_{\sigma\sigma}}, \quad R \equiv 1 - \frac{\chi_{\sigma\sigma'}}{\chi_{\sigma\sigma}}. \quad (2.16)$$

Here, T^* is a characteristic energy scale of the $SU(N)$ Fermi liquid, for instance, the T -linear specific heat of impurity electrons is scaled in the form $C_{\text{imp}} = \frac{N\pi^2}{12} T/T^*$. The Wilson ratio R corresponds to a dimensionless residual interaction between quasiparticles [60]: we will use the following rescaled Wilson ratio \tilde{K} which is bounded in the range $0 \leq \tilde{K} \leq 1$,

$$\tilde{K} \equiv (N-1)(R-1). \quad (2.17)$$

The differential conductance for $SU(N)$ symmetric quantum dots can be expressed in the following form,

scaling the bias voltage eV by T^* ,

$$\frac{dI}{dV} = N g_0 \left[\sin^2 \delta + C_V^{(2)} \frac{eV}{T^*} - C_V^{(3)} \left(\frac{eV}{T^*} \right)^2 + \dots \right], \quad (2.18)$$

$$g_0 \equiv \frac{e^2}{h} \frac{4\Gamma_L \Gamma_R}{(\Gamma_L + \Gamma_R)^2} = \frac{e^2}{h} (1 - \gamma_{\text{dif}}^2). \quad (2.19)$$

The dimensionless coefficients $C_V^{(2)}$ and $C_V^{(3)}$, can be deduced from the general formulas given in Eqs. (B5) and (B6), taking into account the $SU(N)$ symmetry:

$$C_V^{(2)} = \frac{\pi}{4} \left[\alpha_{\text{dif}} (1 - \tilde{K}) - \gamma_{\text{dif}} \tilde{K} \right] \sin 2\delta. \quad (2.20)$$

For $N = 2$, this reproduces the previous result obtained by Aligia for the spin-1/2 Anderson model [56, 57]. $C_V^{(2)}$ consists of a linear combination of α_{dif} and γ_{dif} , and it identically vanishes $C_V^{(2)} \rightarrow 0$ when both the tunnel couplings and the bias voltages are symmetrical $\alpha_{\text{dif}} = \gamma_{\text{dif}} = 0$. The magnitude is determined also by \tilde{K} and $\sin 2\delta$ which can be related to the derivative of the spectral function ρ'_d , given in Eq. (2.12): $\sin 2\delta/T^* = 4\Delta\rho'_d$. Furthermore, $C_V^{(2)}$ is an odd function of ξ_d . Note that $C_V^{(2)}$ depends on the Coulomb interaction only through the real part of the self-energy.

In contrast, $C_V^{(3)}$ given in the following depends on both the real part that determines the high-order energy shifts and imaginary part that destroy phase coherence [61, 62], specifically on the order ω^2 and $(eV)^2$ terms. The exact formula of the coefficient $C_V^{(3)}$ for order $(eV)^3$ nonlinear current is composed of two parts: W_V and Θ_V which represent the two-body contribution and three-body one, respectively,

$$C_V^{(3)} = \frac{\pi^2}{64} (W_V + \Theta_V), \quad (2.21)$$

$$W_V \equiv -\cos 2\delta \left[1 + 3\alpha_{\text{dif}}^2 - 6(\alpha_{\text{dif}}^2 + \alpha_{\text{dif}}\gamma_{\text{dif}}) \tilde{K} + \left\{ \frac{5}{N-1} + 3\alpha_{\text{dif}}^2 + 6\alpha_{\text{dif}}\gamma_{\text{dif}} + \frac{3(N-2)}{N-1} \gamma_{\text{dif}}^2 \right\} \tilde{K}^2 \right], \quad (2.22)$$

$$\Theta_V \equiv \left[1 + 3\alpha_{\text{dif}}^2 \right] \Theta_I + 3 \left[1 + 3\alpha_{\text{dif}}^2 + 4\alpha_{\text{dif}}\gamma_{\text{dif}} \right] \tilde{\Theta}_{\text{II}} + 6 \left[\alpha_{\text{dif}}^2 + 2\alpha_{\text{dif}}\gamma_{\text{dif}} + \gamma_{\text{dif}}^2 \right] \tilde{\Theta}_{\text{III}}. \quad (2.23)$$

$C_V^{(3)}$ depends on the asymmetry parameters through the quadratic terms, i.e., α_{dif}^2 , $\alpha_{\text{dif}}\gamma_{\text{dif}}$, and γ_{dif}^2 . Effects of the three-body corrections enter through the dimension-

less parameters:

$$\Theta_I \equiv \frac{\sin 2\delta}{2\pi} \frac{\chi_{\sigma\sigma\sigma}^{[3]}}{\chi_{\sigma\sigma}^2}, \quad (2.24)$$

$$\tilde{\Theta}_{\text{II}} \equiv (N-1) \frac{\sin 2\delta}{2\pi} \frac{\chi_{\sigma\sigma'\sigma'}^{[3]}}{\chi_{\sigma\sigma}^2}, \quad (2.25)$$

$$\tilde{\Theta}_{\text{III}} \equiv \frac{(N-1)(N-2)}{2} \frac{\sin 2\delta}{2\pi} \frac{\chi_{\sigma\sigma'\sigma''}^{[3]}}{\chi_{\sigma\sigma}^2}, \quad (2.26)$$

for $\sigma \neq \sigma' \neq \sigma'' \neq \sigma$. In particular, $\tilde{\Theta}_{\text{III}}$ represents the correlation between three different levels which appears for $N \geq 3$. This component $\tilde{\Theta}_{\text{III}}$ will give no contribution to $C_V^{(3)}$ through Eq. (2.23) if there is no tunnel or bias asymmetry [44, 63]: W_V and Θ_V take the following form at $\alpha_{\text{dif}} = \gamma_{\text{dif}} = 0$,

$$W_V \xrightarrow{\alpha_{\text{dif}}=\gamma_{\text{dif}}=0} -\cos 2\delta \left(1 + \frac{5\tilde{K}^2}{N-1} \right), \quad (2.27)$$

$$\Theta_V \xrightarrow{\alpha_{\text{dif}}=\gamma_{\text{dif}}=0} \Theta_I + 3\tilde{\Theta}_{\text{II}}. \quad (2.28)$$

When both the chemical potentials and the tunnel couplings are inverted such that $(\alpha_{\text{dif}}, \gamma_{\text{dif}}) \rightarrow (-\alpha_{\text{dif}}, -\gamma_{\text{dif}})$, the coefficients $C_V^{(2)}$ and $C_V^{(3)}$ exhibit odd and even properties, respectively: $C_V^{(2)} \rightarrow -C_V^{(2)}$ and $C_V^{(3)} \rightarrow C_V^{(3)}$ as shown in Appendix B. These formulas of $C_V^{(2)}$ and $C_V^{(3)}$ of the Anderson model for arbitrary level structures $\epsilon_{d\sigma}$ are consistent, in the limit of strong interaction $U \rightarrow \infty$, with the corresponding formulas for the $SU(N)$ Kondo model obtained by Mora *et al.* [40] at integer-filling points $\langle n_d \rangle = 1, 2, \dots, N-1$, with $n_d \equiv \sum_{\sigma} n_{d\sigma}$.

III. NRG RESULTS FOR FERMILIQUID PARAMETERS

In this section, we summarize the basic properties of quasiparticles in the $SU(4)$ and $SU(6)$ symmetric cases. Specifically, we have calculated the Fermi-liquid parameters δ , $\chi_{\sigma\sigma'}$, and $\chi_{\sigma\sigma'\sigma''}^{[3]}$ with the NRG approach, dividing N channels into $N/2$ pairs, and using the $SU(2)$ spin and $U(1)$ charge symmetries for each pair, i.e., totally $\prod_{k=1}^{N/2} [SU(2) \otimes U(1)]_k$ symmetries. The discretization parameter Λ and the number of low-lying energy states N_{trunc} are chosen such that $(\Lambda, N_{\text{trunc}}) = (6, 10000)$ for $N = 4$, and $(20, 30000)$ for $N = 6$ [44]. The phase shift and renormalized parameters have been deduced from the energy flow of NRG [48, 64–67].

A. $SU(4)$ Fermi-liquid properties

1. Two-body correlation functions of an $SU(4)$ dot

The Fermi-liquid parameters of an $SU(4)$ quantum dot, which can be deduced from the phase shift and the linear

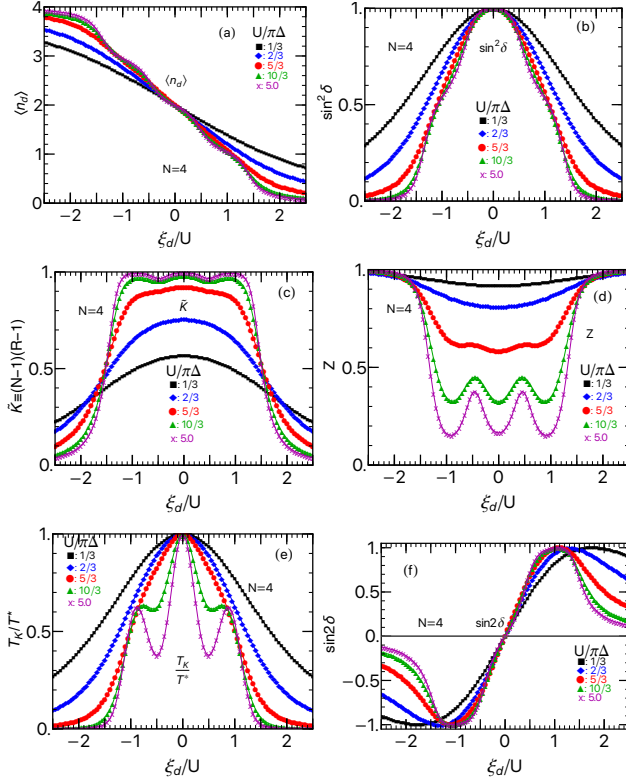


FIG. 1. Fermi-liquid parameters of an SU(4) dot are plotted as a function of ξ_d/U for $U/(\pi\Delta) = 1/3, 2/3, 5/3, 10/3, 5.0$: (a) $\langle n_d \rangle$, (b) $\sin^2 \delta$, (c) rescaled Wilson ratio $\tilde{K} \equiv (N-1)(R-1)$, (d) renormalized factor z , (e) T_K/T^* , and (f) $\sin 2\delta$. Here, T_K is defined as the value of $T^* \equiv 1/(4\chi_{\sigma\sigma})$ at half filling $\xi_d = 0$.

susceptibilities, are shown in Fig. 1 as a function of ξ_d for several different values of $U/(\pi\Delta) = 1/3, 2/3, 5/3, 10/3, 5$. For large $U/(\pi\Delta) \gtrsim 2.0$, the occupation number in Fig. 1(a) shows a Coulomb-staircase behavior with the plateaus of integer height $\langle n_d \rangle \simeq 1.0, 2.0, 3.0$ and the steps at $\xi_d \simeq -U, 0, U$: the structure becomes clearer for stronger interactions. Figure 1(b) shows $\sin^2 \delta$ corresponding to the linear term of the differential conductance in Eq. (1.1). For strong interactions $U/(\pi\Delta) \gtrsim 2.0$, the Kondo ridges which reflect the step structure of the occupation number of the values $\langle n_d \rangle \simeq 1, 2, 3$ evolve at $\xi_d \simeq U, 0, -U$, respectively, as U increases.

Figure 1(c) shows the rescaled Wilson ratio $\tilde{K} \equiv (N-1)(R-1)$. It has a wide plateau that reaches the strong-coupling limit value $\tilde{K} \simeq 1$ in the region $-1.5U \lesssim \xi_d \lesssim 1.5U$, for large interactions $U/(\pi\Delta) \gtrsim 3.0$. This is caused by the fact that charge fluctuations are suppressed in this region and it makes the charge susceptibility vanish: $\chi_c \propto \chi_{\sigma\sigma} + (N-1)\chi_{\sigma\sigma'} \rightarrow 0$. The shallow dips of \tilde{K} at $\xi_d \simeq \pm 0.5U$ is caused by the charge fluctuations at the steps of the Coulomb staircase structure of $\langle n_d \rangle$.

Correspondingly, the renormalization factor z in Fig. 1(d) exhibits a broad valley structure at $-1.5U \lesssim \xi_d \lesssim$

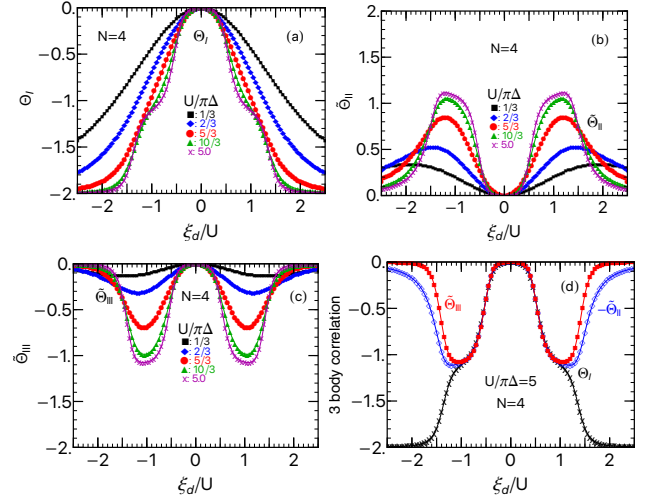


FIG. 2. Three-body correlation functions of an SU(4) dot plotted vs ξ_d/U for $U/\pi\Delta = 1/3, 2/3, 5/3, 10/3, 5.0$: (a) Θ_I , (b) Θ_{II} , (c) Θ_{III} . (d) comparison of Θ_I , $-\Theta_{II}$, and Θ_{III} at a large interaction $U/(\pi\Delta) = 5.0$. It indicates that $\Theta_I \simeq -\Theta_{II} \simeq \Theta_{III}$ over a wide range of $-U \lesssim \xi_d \lesssim U$.

$1.5U$, which becomes deeper as U increases. It has a clear local minimum for $U/(\pi\Delta) \gtrsim 2.0$ at $\xi_d \simeq 0$ and $\pm U$, where $\langle n_d \rangle$ takes integer values: it also has a local maximum at intermediate valence states in between the two adjacent minima. Figure 1(e) shows the gate voltage ξ_d dependence of the inverse of the characteristic energy scale, $1/T^*$, scaled by T_K that is defined as the value of T^* at the electron-hole symmetric point $\xi_d = 0$. It shows an oscillatory behavior for strong interactions $U \gtrsim 3.0$, reflecting the dependence of z on ξ_d . In particular, $1/T^*$ reaches a local maximum at the integer-filling points where the SU(4) Kondo effect occurs.

Some of the two-body correlation functions contribute to the low-energy transport through the derivative of the impurity density of state: $\rho'_d = (\chi_{\sigma\sigma}/\Delta) \sin 2\delta$ given in Eq. (2.12). For instance, the coefficient $C_V^{(2)}$ is proportional to ρ'_d . Figure 1(f) shows $\sin 2\delta$. It is an odd function of ξ_d and vanishes at $\xi_d = 0$ where the phase shift takes the value $\delta = \pi/2$. For strong interactions $U/(\pi\Delta) \gtrsim 3.0$, it has a wide maximum (minimum) at $\xi_d \simeq U$ ($-U$), where the 1/4-filling (3/4-filling) SU(4) Kondo occurs.

2. Three-body correlation functions of an SU(4) dot

We next consider the three-body correlations between electrons passing through an SU(4) symmetric dot. Figure 2 shows Θ_I , Θ_{II} , and Θ_{III} as a function of ξ_d/U for several different values of U . These dimensionless three-body correlation functions vanish in the electron-hole symmetric case $\xi_d = 0$. For strong interactions $U/(\pi\Delta) \gtrsim 3.0$, a plateau of the width U emerges at

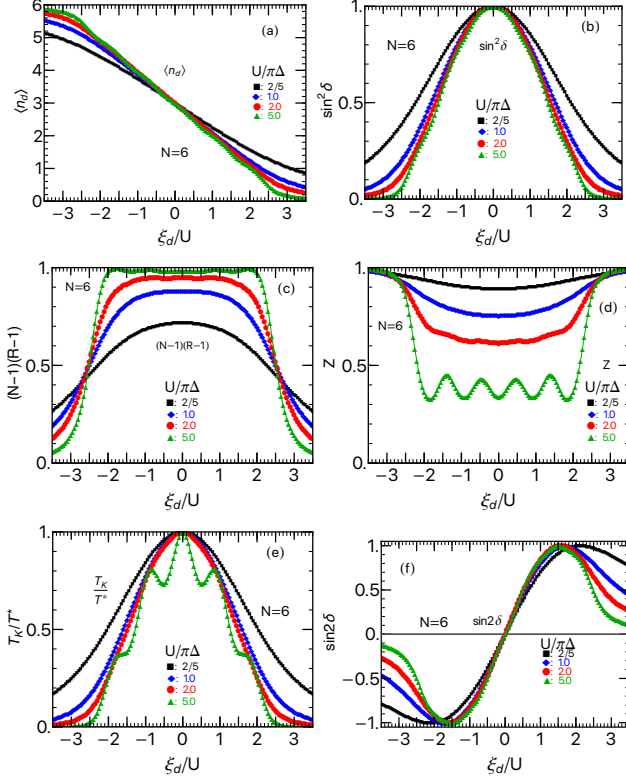


FIG. 3. Fermi-liquid parameters of an SU(6) dot are plotted as a function of ξ_d/U for $U/(\pi\Delta) = 2/5, 1.0, 2.0, 5.0$. (a) $\langle n_d \rangle$, (b) $\sin^2 \delta$, (c) rescaled Wilson ratio $\tilde{K} \equiv (N-1)(R-1)$, (d) renormalized factor z , (e) T_K/T^* , and (f) $\sin 2\delta$. Here, T_K is defined as the value of $T^* \equiv 1/(4\chi_{\sigma\sigma})$ at half filling $\xi_d = 0$.

$\xi_d \simeq 0$ and $\pm U$, i.e., at integer filling points $\langle n_d \rangle \simeq 1, 2, 3$. The plateau structure evolves further as interaction U increases. Specifically, the correlation function between three different levels $\tilde{\Theta}_{III}$ appears for SU(N) quantum dots with $N \geq 3$, and contributes to the nonlinear conductance when there are some asymmetries in the tunnel couplings or the bias voltages.

A comparison of the three independent components Θ_I , $-\tilde{\Theta}_{II}$, and $\tilde{\Theta}_{III}$ is made in Fig. 2(d) for a large interaction $U/(\pi\Delta) = 5.0$. It shows that these three components approach each other very closely over a wide range of gate voltages $-1.5U \lesssim \xi_d \lesssim 1.5U$,

$$\Theta_I \simeq -\tilde{\Theta}_{II} \simeq \tilde{\Theta}_{III}. \quad (3.1)$$

This is caused by the fact that the derivatives of the two independent components of linear susceptibilities, $|\frac{\partial\chi_{\sigma\sigma'}}{\partial\epsilon_d}|$ and $|\frac{\partial\chi_{\sigma\sigma}}{\partial\epsilon_d}|$, become much smaller than an inverse of the characteristic energy scale $(T^*)^{-2}$ in a wide range of electron fillings $1 \lesssim \langle n_d \rangle \lesssim N-1$, in addition to the suppression of the charge fluctuations $\chi_c \simeq 0$, mentioned above [see Appendix C] [44].

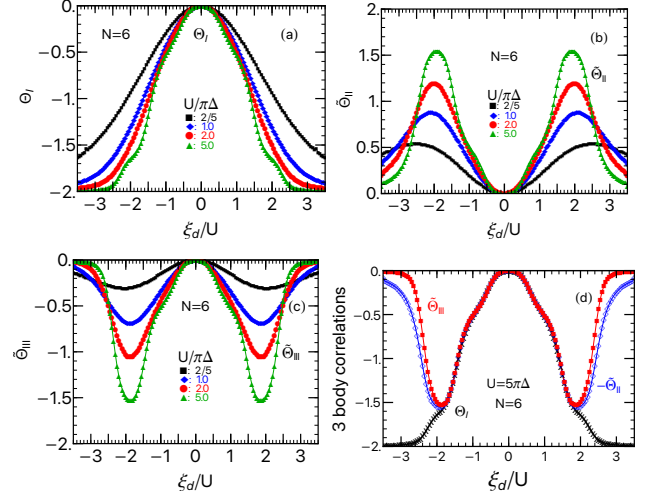


FIG. 4. Three-body correlation functions of an SU(6) dot plotted vs ξ_d/U for $U/\pi\Delta = 2/5, 1.0, 2.0, 5.0$: (a) Θ_I , (b) $-\tilde{\Theta}_{II}$, (c) $\tilde{\Theta}_{III}$. (d) comparison of Θ_I , $-\tilde{\Theta}_{II}$, and $\tilde{\Theta}_{III}$ at a large interaction $U/(\pi\Delta) = 5.0$. It indicates that $\Theta_I \simeq -\tilde{\Theta}_{II} \simeq \tilde{\Theta}_{III}$ over a wide range of $-(N-1)/2U \lesssim \xi_d \lesssim (N-1)/2$ for $N = 6$.

B. SU(6) Fermi-liquid properties

1. Two-body correlation functions for an SU(6) dot

We next summarize the low-energy Fermi-liquid properties of SU(6) quantum dots. The phase shift and the renormalized parameters that can be deduced from the two-body correlations are plotted as a function of the gate voltage ξ_d/U in Fig. 3, for several different values of $U/(\pi\Delta) = 2/5, 1.0, 2.0, 5.0$, i.e., from weak to strong interactions. The behaviors of these parameters are similar to those of the SU(4) quantum dots. However, the number of different SU(N) Kondo states occurring at integer fillings increases with N , i.e., $\langle n_d \rangle = 1, 2, \dots, N-1$. It takes place at $\xi_d \simeq 0.0, \pm U, \dots, \pm \frac{N-2}{2}U$, and gives an interesting variety in low-energy transport. As N increases, quantum fluctuations caused by the Coulomb interaction U is suppressed, and in particular, the mean-field theory becomes exact in the large N limit of the finite- U Anderson impurity model [68]. Hence for larger N , electron-correlation effects reveal stronger interactions U .

In Fig. 3(a), we can see that the Coulomb staircase behavior of the occupation number $\langle n_d \rangle$ emerges for a large interaction $U/(\pi\Delta) = 5.0$, which has steps at $\xi_d \simeq 0.0, \pm U, \pm 2U$ for SU(6) quantum dots. The transmission probability $\sin^2 \delta$, shown in Fig. 3(b), reaches the unitary limit value $\sin^2 \delta = 1.0$ at half filling $\xi_d = 0$. We can see that the plateau structure develops as U increases, and it becomes visible at a strong interaction $U/(\pi\Delta) = 5.0$.

Figure 3(c) shows that the rescaled Wilson ratio \tilde{K} for $N = 6$ has a wide flat peak at $-(N-1)U/2 \lesssim \xi_d \lesssim (N-1)U/2$, the height of which increases with

U . In particular, it approaches saturation value $\tilde{K} \simeq 1$ at $U/(\pi\Delta) = 5.0$ due to the suppression of charge fluctuations, as mentioned.

The renormalization factor z for SU(6) quantum dots, shown in Fig. 3(d), exhibits a broad valley structure similar to the one for the SU(4) symmetric case. The valley becomes deeper as U increases, and the local minima emerge at the integer-filling points, reflecting the electron correlations due to the SU(6) Kondo effects. Figure 3(e) shows that the inverse of the characteristic energy $1/T^*$, which is scaled by the value T_K defined at half filling $\xi_d = 0$. It has peaks situated at $\xi_d \simeq 0, \pm U, \pm 2U$ for a strong interaction $U/(\pi\Delta) = 5.0$, although the ones at $\pm 2U$ are still developing. These peaks correspond to the SU(6) Kondo temperature at each of the integer-filling points.

Figure 3(f) shows $\sin 2\delta$ for $N = 6$, which is proportional to the derivative of the density of states $\rho'_d = (\chi_{\sigma\sigma}/\Delta) \sin 2\delta$, and determines the magnitude of the coefficient $C_V^{(2)}$ of the nonlinear current, as mentioned. This factor $\sin 2\delta$ is an odd function of ξ_d , and at a strong interaction $U/(\pi\Delta) = 5.0$ it takes a broad peak (dip) at $\delta = \pi/4$ ($3\pi/4$) corresponding to the half-integer filling $\langle n_d \rangle = 1.5$ (4.5) where charge fluctuations are not fully suppressed.

2. Three-body correlation functions of an SU(6) dot

Figure 4 shows three-body correlations between electrons passing through an SU(6) quantum dot, calculated as a function of ξ_d for several values of interactions $U/\pi\Delta = 2/5, 1.0, 2.0, 5.0$. These dimensionless correlation functions $\Theta_I, \tilde{\Theta}_{II},$ and $\tilde{\Theta}_{III}$ vanish at half filling $\xi_d = 0$, and away from half filling, they are enhanced as U increases. We can see that for a strong interaction $U/(\pi\Delta) = 5.0$ there emerges either a wide peak, a wide dip, or a plateau at $\xi_d \simeq \pm U, \pm 2U$, i.e., at integer filling points. The component between three different levels $\tilde{\Theta}_{III}$ also contributes to the order $(eV)^3$ term of nonlinear current through an SU(6) quantum dot when there are some asymmetries in the tunnel couplings or the bias voltages.

In Fig. 4(d) the three independent components $\Theta_I, -\tilde{\Theta}_{II},$ and $\tilde{\Theta}_{III}$ are compared in a strong interaction case $U/(\pi\Delta) = 5.0$. It shows that these three components approach each other very closely $\Theta_I \simeq -\tilde{\Theta}_{II} \simeq \tilde{\Theta}_{III}$ over a wide range of the gate voltage $-(N-1)U/2 \lesssim \xi_d \lesssim (N-1)U/2$ with $N = 6$. This is due to the fact that the diagonal component $\chi_{\sigma\sigma\sigma}^{[3]}$ dominates the three-body correlation, and the derivatives $|\frac{\partial\chi_{\sigma\sigma}}{\partial\epsilon_d}|$ and $|\frac{\partial\chi_{\sigma\sigma'}}{\partial\epsilon_d}|$ become much smaller than $(T^*)^{-2}$ in a wide range of electron fillings $1 \lesssim \langle n_d \rangle \lesssim N-1$ [see Appendix C] [44].

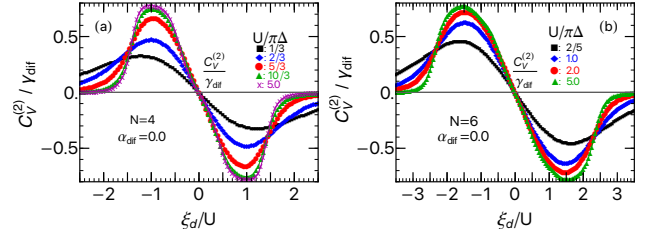


FIG. 5. Effects of tunnel asymmetry γ_{dif} on order $(eV)^2$ nonlinear current: $C_V^{(2)}/\gamma_{\text{dif}}$ given by Eq. (4.3) for symmetrical bias voltages $\alpha_{\text{dif}} = 0.0$ is plotted vs ξ_d/U , varying interactions from weak to strong. (a) for SU(4) quantum dots with $U/(\pi\Delta) = 1/3, 2/3, 5/3, 10/3, 5.0$. (b) for SU(6) quantum dots with $U/(\pi\Delta) = 2/5, 1.0, 2.0, 5.0$.

IV. ORDER $(eV)^2$ NONLINEAR CURRENT FOR SU(4) AND SU(6) CASES

The coefficient $C_V^{(2)}$, defined in Eqs. (2.18) and (2.20), emerges when the tunnel coupling or the bias voltage is not symmetric. Its magnitude is determined by the Wilson ratio \tilde{K} and the derivative of the density of states: $\rho'_d = (\chi_{\sigma\sigma}/\Delta) \sin 2\delta$.

In this section, we first of all describe behavior of $C_V^{(2)}$ in some limiting cases, and then discuss the NRG results to show how the coefficient evolves with the tunnel and bias asymmetries.

A. Behavior of $C_V^{(2)}$ in some limiting cases

We have seen in Figs. 1 and 3 that the Wilson ratio reaches the saturation value $\tilde{K} \simeq 1$ over a wide range of gate voltages $-(N-1)U/2 \lesssim \xi_d \lesssim (N-1)U/2$ for large U , where the quantum dot is partially filled $1 \lesssim \langle n_d \rangle \lesssim N-1$. This is caused by the fact that the charge fluctuations are significantly suppressed in this region, as mentioned. In the limit of strong interactions, $C_V^{(2)}$ becomes independent of the bias asymmetry α_{dif} :

$$C_V^{(2)} \xrightarrow{\tilde{K} \rightarrow 1} -\frac{\pi}{4} \gamma_{\text{dif}} \sin 2\delta, \quad (4.1)$$

In contrast, in the limit of $|\xi_d| \rightarrow \infty$ where $\langle n_d \rangle$ approaches 0 or N , the Wilson ratio approaches the non-interacting value $\tilde{K} \rightarrow 0$, and $C_V^{(2)}$ becomes independent of tunnel asymmetry γ_{dif} :

$$C_V^{(2)} \xrightarrow{\tilde{K} \rightarrow 0} \frac{\pi}{4} \alpha_{\text{dif}} \sin 2\delta. \quad (4.2)$$

B. Effects of tunnel asymmetry $\gamma_{\text{dif}} \neq 0$ on $C_V^{(2)}$ for symmetric bias voltages $\alpha_{\text{dif}} = 0$

We first of all consider effects of tunneling asymmetries γ_{dif} on $C_V^{(2)}$, taking bias voltages to be symmetric $\alpha_{\text{dif}} =$

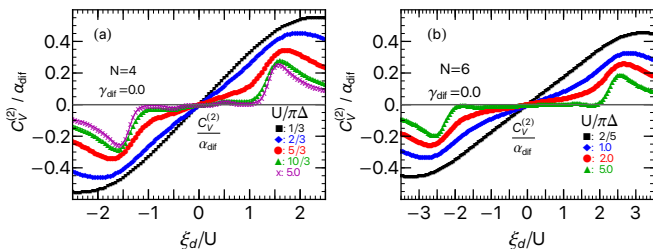


FIG. 6. Effects of bias-voltage asymmetry α_{dif} on order $(eV)^2$ nonlinear current: $C_V^{(2)}/\alpha_{\text{dif}}$ given by Eq. (4.4) for symmetric junctions with $\gamma_{\text{dif}} = 0.0$ is plotted vs ξ_d/U , varying interactions from weak to strong. (a) for SU(4) quantum dots with $U/(\pi\Delta) = 1/3, 2/3, 5/3, 10/3, 5.0$. (b) for SU(6) quantum dots with $U/(\pi\Delta) = 2/5, 1.0, 2.0, 5.0$.

0:

$$C_V^{(2)} \xrightarrow{\alpha_{\text{dif}}=0} -\frac{\pi}{4} \gamma_{\text{dif}} \tilde{K} \sin 2\delta. \quad (4.3)$$

In this case, $C_V^{(2)}$ is proportional to γ_{dif} , and is determined by \tilde{K} and $\sin 2\delta$. Figure 5 shows $C_V^{(2)}/\gamma_{\text{dif}}$ as a function of ξ_d/U for symmetric bias voltages $\alpha_{\text{dif}} = 0.0$. We have examined the behaviors from weak to strong interactions: (a) for SU(4) quantum dots with $U/(\pi\Delta) = 1/3, 2/3, 5/3, 10/3, 5.0$, and (b) for SU(6) quantum dots with $U/(\pi\Delta) = 2/5, 1.0, 2.0, 5.0$.

As U increases, a wide peak and a wide dip of $C_V^{(2)}$ evolve at $\xi_d \simeq U/4$ and $-U/4$, where the occupation number reaches the value of $\langle n_d \rangle \simeq N/4$ and $3N/4$, respectively. It corresponds to phase shifts of $\delta \simeq \pi/4$ and $3\pi/4$, at which $\sin 2\delta$ takes an extreme value as seen in Figs. 1(f) and 3(f). The peak and dip structures also reflect the fact that the Wilson ratio is almost saturated $\tilde{K} \simeq 1.0$ in a wider range of $|\xi_d| \lesssim (N-1)U/2$ for large U in Figs. 1(c) and 3(c). The Kondo effect of an integer filling occurs at the flat peak and the flat dip for $N = 4$ quantum dots. In contrast, for $N = 6$, it is an intermediate valence state that occurs at the peak and dip, and thus the structures become round rather than flat since charge fluctuations remain active.

Outside the correlated region, the absolute value of $C_V^{(2)}$ decreases as U increases, for both $N = 4$ and 6 in Figs. 5 (a) and (b), respectively. In particular, at $|\xi_d| \gg (N-1)U/2$, it vanishes asymptotically $C_V^{(2)} \rightarrow 0$ as the occupation number approaches $\langle n_d \rangle \rightarrow 0$ or N .

C. Effects of bias asymmetry $\alpha_{\text{dif}} \neq 0$ on $C_V^{(2)}$ for symmetric tunnel junctions $\gamma_{\text{dif}} = 0$

We next consider the effects of bias asymmetries α_{dif} on $C_V^{(2)}$, setting tunnel junctions to be symmetric $\gamma_{\text{dif}} = 0$. In this case, $C_V^{(2)}$ becomes proportional to α_{dif} , as

$$C_V^{(2)} \xrightarrow{\gamma_{\text{dif}}=0} \frac{\pi}{4} \alpha_{\text{dif}} (1 - \tilde{K}) \sin 2\delta. \quad (4.4)$$

The ratio $C_V^{(2)}/\alpha_{\text{dif}}$ for this case is plotted vs ξ_d/U in Fig. 6. We have also examined from weak to strong interactions for symmetric tunnel couplings $\gamma_{\text{dif}} = 0.0$: (a) for SU(4) quantum dots with $U/(\pi\Delta) = 1/3, 2/3, 5/3, 10/3, 5.0$, and (b) for SU(6) quantum dots with $U/(\pi\Delta) = 2/5, 1.0, 2.0, 5.0$.

At $|\xi_d| \lesssim (N-1)U/2$, where the localized levels of quantum dots are partially filled $1 \lesssim \langle n_d \rangle \lesssim N-1$, the factor $1 - \tilde{K}$ in Eq. (4.4) becomes very small as U increases since the Wilson ratio approaches the saturation value $\tilde{K} \rightarrow 1.0$. Therefore, $C_V^{(2)}$ almost vanishes in this region for strong interactions $U/(\pi\Delta) \gtrsim 3.0$. However, weak oscillatory behavior survives at $\xi_d/U \simeq \pm(N-1-2m)/2$ for $m = 1, \dots, N/2-1$, and it is caused by charge fluctuations in the intermediate valence states between two adjacent integer filling points.

In contrast outside the correlated region, at $|\xi_d| \gg (N-1)U/2$, the rescaled Wilson ratio decreases and it eventually vanishes in the limit of $|\xi_d| \rightarrow \infty$ as shown in Figs. 1(c) and 3(c), so that $1 - \tilde{K} \rightarrow 1.0$ in Eq. (4.4). Therefore, the behavior of $C_V^{(2)}$ in this region is mainly determined by the other factor $\sin 2\delta$. The localized levels of quantum dots become almost empty or fully occupied in the limit of $|\xi_d| \rightarrow \infty$. Correspondingly, at the crossover region $|\xi_d| \simeq (N-1)U/2$, the phase shift takes the value around $\delta \simeq \pi/N$ at $\xi_d \simeq (N-1)U/2$, and $\delta \simeq \pi(N-1)/N$ at $\xi_d \simeq -(N-1)U/2$. Thus, the peak height, or the dip depth, of $C_V^{(2)}$ decreases as N increases: the amplitude becomes larger for the SU(4) quantum dots than the SU(6) in Fig. 6.

For weak interactions, effects of bias asymmetries α_{dif} appear in the whole region of ξ_d , particularly $C_V^{(2)}$ takes finite values in the region of $|\xi_d| \simeq (N-1)U/2$.

D. $C_V^{(2)}$ under both asymmetries $\alpha_{\text{dif}} \neq 0$ and $\gamma_{\text{dif}} \neq 0$

We next consider the behavior of $C_V^{(2)}$ in the presence of both asymmetries, i.e., $\alpha_{\text{dif}} \neq 0$ and $\gamma_{\text{dif}} \neq 0$. We have seen above that in the strongly correlated region at $|\xi_d| \lesssim (N-1)U/2$ for large U , the coefficient $C_V^{(2)}$ is given by Eq. (4.1) and it becomes almost independent of bias asymmetries α_{dif} , since the Wilson ratio approaches $\tilde{K} \simeq 1.0$. Conversely, $C_V^{(2)}$ is given by Eq. (4.2), which does not depend on tunnel asymmetries γ_{dif} , for small U or outside the correlated region as $\tilde{K} \simeq 0.0$. These properties provide the key to clarify overall characteristics of $C_V^{(2)}$ in a wide parameter range.

1. Effects of bias asymmetry $\alpha_{\text{dif}} \neq 0$ on $C_V^{(2)}$ at large tunnel asymmetry γ_{dif} ($\Gamma_L \gg \Gamma_R$)

The coefficient $C_V^{(2)}$ for a large fixed tunnel asymmetry $\gamma_{\text{dif}} = 0.8$, is plotted vs ξ_d in Fig. 7, varying bias asymme-

tries, $\alpha_{\text{dif}} = 0.0, \pm 0.5, \pm 1.0$. The upper panels describe the behavior for a strong interaction $U/(\pi\Delta) = 5.0$, and the lower ones describe that for weak interactions, i.e., $U/(\pi\Delta) = 1/3$ for SU(4), and $U/(\pi\Delta) = 2/5$ for SU(6).

The results in Figs. 7 (a) and (b) show that the coefficient $C_V^{(2)}$ becomes almost independent of bias asymmetries in the strong coupling region $|\xi_d| \lesssim (N-1)U/2$ for large U since the Wilson ratio approaches the saturated value $\tilde{K} \simeq 1.0$. In this region, $C_V^{(2)}$ is proportional to γ_{dif} , and shows the same behavior as that in Figs. 5(a) and (b). For $N \geq 4$, $C_V^{(2)}$ has a peak and a dip which correspond to the points $\sin 2\delta \simeq \pm 1.0$ inside the correlated region, and thus the coefficient takes the value $C_V^{(2)} \simeq \pm(\pi/4)\gamma_{\text{dif}}$ at the extreme points. This kind of extreme points in the correlated region do not take place for SU(2) quantum dots since, for $N = 2$, the phase shift takes the values $\delta = \pi/4$ and $3\pi/4$ in the valence fluctuation regime, instead of the Kondo regime [55]. Around the extreme points, $C_V^{(2)}$ takes a typical flat structure of the Kondo state for $N = 4$, while it takes a round structure typical to the intermediate valence state for $N = 6$, as mentioned above.

The coefficient $C_V^{(2)}$ has an additional zero point other than the one at $\xi_d = 0$ in the case $\alpha_{\text{dif}}\gamma_{\text{dif}} > 0$, at which bias and tunneling asymmetries cooperatively enhance the charge transfer from one of the electrodes, and the Wilson ratio satisfies the following condition,

$$\tilde{K} = \frac{\alpha_{\text{dif}}}{\alpha_{\text{dif}} + \gamma_{\text{dif}}}. \quad (4.5)$$

It represents the condition that the first and second terms in Eq. (2.20) cancel each other out. It takes place valence fluctuation regime $|\xi_d| \gtrsim (N-1)U/2$ in Fig. 7. Conversely, effects of tunnel and bias asymmetries become constructive for $\alpha_{\text{dif}}\gamma_{\text{dif}} < 0.0$. The behavior at $|\xi_d| \gg (N-1)U/2$, is determined by the factor $\alpha_{\text{dif}} \sin 2\delta$.

2. Effects of tunnel asymmetry $\gamma_{\text{dif}} \neq 0$ on $C_V^{(2)}$ at large bias asymmetry $\alpha_{\text{dif}} = 1$

We next consider the effects of tunnel asymmetry γ_{dif} on $C_V^{(2)}$ at large bias asymmetry $\alpha_{\text{dif}} = 1.0$, which describes the situation that the right lead is grounded. Figure 8 shows the result of $C_V^{(2)}$, plotted as a function ξ_d varying tunnel asymmetries, as $\gamma_{\text{dif}} = 0.0, \pm 0.2, \pm 0.5, \pm 0.8$: (top panels) for a strong $U/(\pi\Delta) = 5.0$, and (bottom panels) for weak interactions with (left panels) $U/(\pi\Delta) = 1/3$ for SU(4) quantum dots and (right panels) $U/(\pi\Delta) = 2/5$ for SU(6) ones.

In the strong-coupling limit region $|\xi_d| \lesssim (N-1)U/2$, the results in Figs. 8 (a) and (b) show almost the same behavior as that for symmetric bias voltage $\alpha_{\text{dif}} = 0.0$ given in Figs. 5 (a) and (b), respectively, except for the ones for $\gamma_{\text{dif}} = 0.0$. This is because the Wilson ratio reaches saturated $\tilde{K} \simeq 1.0$ and $C_V^{(2)}$ becomes independent of α_{dif} , as shown in Eq. (4.1).

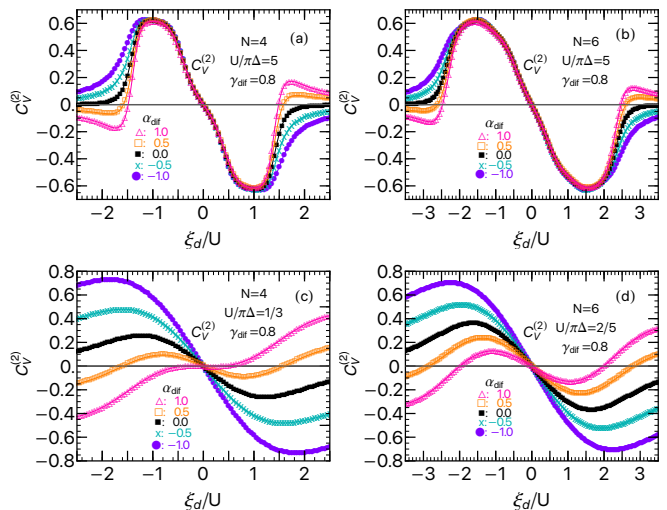


FIG. 7. $C_V^{(2)}$ for a junction with large tunnel asymmetry $\gamma_{\text{dif}} = 0.8$ is plotted vs ξ_d/U , varying bias-voltage asymmetries, as $\alpha_{\text{dif}} = -1.0$ (\bullet), -0.5 (\times), 0.0 (\blacksquare), 0.5 (\square), 1.0 (\triangle). (Left panels) for SU(4) quantum dots and (Right panels) for SU(6) ones, with (top panels) a strong interaction $U/(\pi\Delta) = 5.0$ and with (bottom panels) weak interactions $U/(\pi\Delta) = 1/3$ for SU(4) and $U/(\pi\Delta) = 2/5$ for SU(6).

In the valence fluctuation region $|\xi_d| \simeq (N-1)U/2$, $C_V^{(2)}$ has an extra zero point other than the one at $\xi_d = 0$ in the case at which $\alpha_{\text{dif}}\gamma_{\text{dif}} > 0$, mentioned above at Eq. (4.5). As the impurity level deviates further away from the electron-hole symmetric point, i.e., at $|\xi_d| \gtrsim (N-1)U/2$, the coefficient $C_V^{(2)}$ becomes less sensitive to γ_{dif} and its behavior is described by Eq. (4.2) as the Wilson ratio approaches $\tilde{K} \simeq 0.0$. We also see in Fig. 8(c) that $C_V^{(2)}$ does not have an extra zero point for SU(4) symmetric quantum dots with a weak interaction. This is because the Wilson ratio in this case takes values in the range $\tilde{K} \lesssim 0.54$ as shown in Fig. 1(c) which does not satisfy the condition Eq. (4.5) as $\alpha_{\text{dif}}/(\alpha_{\text{dif}} + \gamma_{\text{dif}}) \simeq 0.56$ for $\alpha_{\text{dif}} = 1.0$ and $\gamma_{\text{dif}} = 0.8$. Nevertheless, extra zero points will emerge even in this situation if tunnel asymmetries are slightly larger, i.e., $\gamma_{\text{dif}} \gtrsim 0.85$. An example is shown in Fig. 8(d) for SU(6) quantum dots: $C_V^{(2)}$ has an extra zero point clearly for $\gamma_{\text{dif}} = 0.8$, whereas it does not for $\gamma_{\text{dif}} \lesssim 0.5$. In this case, the Wilson ratio is bounded in the range of $\tilde{K} \lesssim 0.72$ as shown in Fig. 3(c), and thus the condition Eq. (4.5) is satisfied for $\gamma_{\text{dif}} = 0.8$ at which $\alpha_{\text{dif}}/(\alpha_{\text{dif}} + \gamma_{\text{dif}}) \simeq 0.56$, whereas it is not, for instance, for $\gamma_{\text{dif}} = 0.2$ as $\alpha_{\text{dif}}/(\alpha_{\text{dif}} + \gamma_{\text{dif}}) \simeq 0.83$.

V. ORDER $(eV)^3$ NONLINEAR CURRENT FOR SU(4) AND SU(6) CASES

The coefficient $C_V^{(3)}$ of the order $(eV)^2$ term of the nonlinear conductance, defined in Eqs. (2.21)–(2.23) has

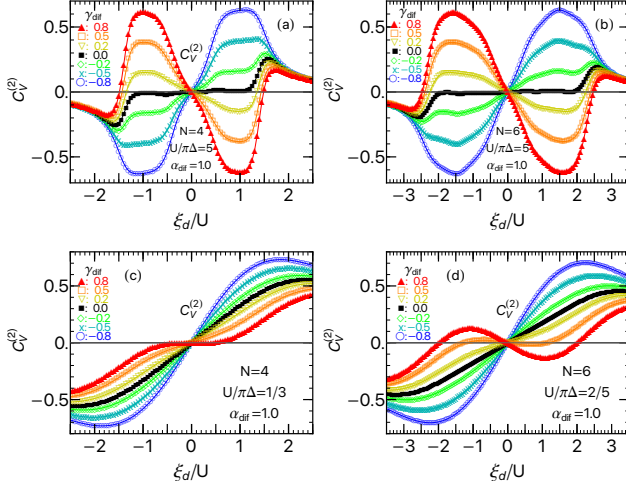


FIG. 8. $C_V^{(2)}$ for a large bias-voltage asymmetry $\alpha_{\text{dif}} = 1.0$ is plotted vs ξ_d , varying tunnel asymmetries, as $\gamma_{\text{dif}} = -0.8$ (\circ), -0.5 (\times), -0.2 (\diamond), 0.0 (\blacksquare), 0.2 (∇), 0.5 (\square) and 0.8 (\triangle). (Left panels) for SU(4) quantum dots and (Right panels) for SU(6) ones, with (top panels) a strong interaction $U/(\pi\Delta) = 5.0$ and (bottom panels) weak interactions $U/(\pi\Delta) = 1/3$ for SU(4) and $U/(\pi\Delta) = 2/5$ for SU(6).

a quadratic dependence on the bias and tunnel asymmetries of the form, α_{dif}^2 , $\alpha_{\text{dif}}\gamma_{\text{dif}}$, and γ_{dif}^2 . In particular, the order γ_{dif}^2 term, which is absent in the SU(2) case [69], emerges for multilevel quantum dots with $N \geq 3$ and plays an important role in the Kondo states with no electron-hole symmetry. In this section, we describe some limiting cases of $C_V^{(3)}$, and then discuss the NRG results for SU(4) and SU(6) quantum dots.

A. Behavior of $C_V^{(3)}$ in some limiting cases

The two-body and three-body parts of $C_V^{(3)}$ defined in Eqs. (2.21)–(2.23) takes the following values in the strong-coupling case where the Wilson ratio reaches the saturated value $\tilde{K} \rightarrow 1.0$ and the three-body correlations functions show the properties $\Theta_I \simeq -\tilde{\Theta}_{II} \simeq \tilde{\Theta}_{III}$ shown in Figs. 1–4,

$$W_V \xrightarrow{\tilde{K} \rightarrow 1} -\cos 2\delta \left[1 + \frac{5}{N-1} + \frac{3(N-2)}{N-1} \gamma_{\text{dif}}^2 \right], \quad (5.1)$$

$$\Theta_V \xrightarrow{\Theta_I \simeq -\tilde{\Theta}_{II} \simeq \tilde{\Theta}_{III}} -2 \left[1 - 3\gamma_{\text{dif}}^2 \right] \Theta_I. \quad (5.2)$$

Our result in this limit is consistent with the corresponding result for the SU(N) Kondo model, given in Eqs. (22) and (32) of Ref. 40. Note that their notation and our one in the strong-interaction limit correspond to each other such that $\alpha_1/(\pi T_K) \Leftrightarrow \chi_{\sigma\sigma}$, and $\alpha_2/(\pi T_K^2) \Leftrightarrow -\frac{1}{2} \chi_{\sigma\sigma}^{[3]}$.

In the limit of $|\xi_d| \rightarrow \infty$, the occupation number reaches $\langle n_d \rangle \rightarrow 0$ or N , and the correlation functions

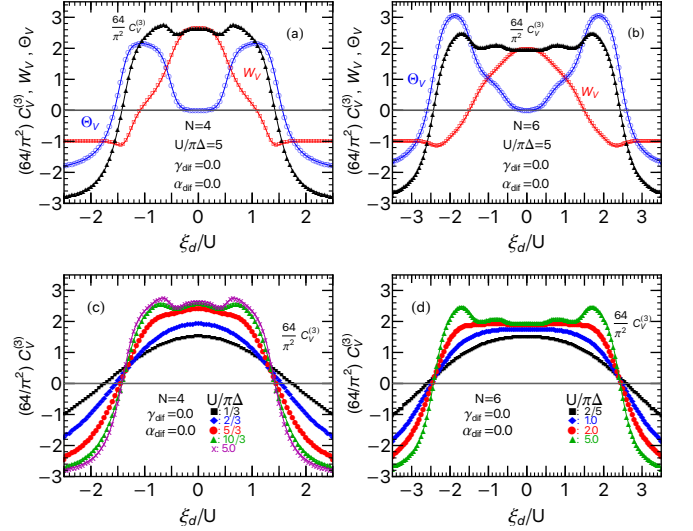


FIG. 9. Coefficient $C_V^{(3)}$ is plotted vs ξ_d/U for the case where both tunnel couplings and bias voltages are symmetric, $\gamma_{\text{dif}} = 0.0$ and $\alpha_{\text{dif}} = 0.0$. Upper panels show the total value of $C_V^{(3)} = (\pi^2/64)(W_V + \Theta_V)$ together with the two-body W_V and three-body Θ_V components, (a) for SU(4) and (b) for SU(6) quantum dots choosing a large interaction $U/(\pi\Delta) = 5.0$. Bottom panels show U dependence of $C_V^{(3)}$: (c) $U/(\pi\Delta) = 1/3, 2/3, 5/3, 10/3, 5.0$ for SU(4), and (d) $U/(\pi\Delta) = 2/5, 1.0, 2.0, 5.0$ for SU(6).

take the noninteracting values, and thus

$$W_V \xrightarrow{|\xi_d| \rightarrow \infty} -(1 + 3\alpha_{\text{dif}}^2), \quad (5.3)$$

$$\Theta_V \xrightarrow{|\xi_d| \rightarrow \infty} -2(1 + 3\alpha_{\text{dif}}^2), \quad (5.4)$$

$$C_V^{(3)} \xrightarrow{|\xi_d| \rightarrow \infty} -\frac{3\pi^2}{64} (1 + 3\alpha_{\text{dif}}^2). \quad (5.5)$$

Note that in this limit, the three-body correlations are given by $\Theta_I \rightarrow -2$, $\tilde{\Theta}_{II} \rightarrow 0$, and $\tilde{\Theta}_{III} \rightarrow 0$ [see Appendix B in Ref. 69].

B. $C_V^{(3)}$ for symmetric tunnel coupling and symmetric bias voltage $\gamma_{\text{dif}} = \alpha_{\text{dif}} = 0$

We describe here previous results obtained for symmetric tunnel coupling and bias voltage $\gamma_{\text{dif}} = \alpha_{\text{dif}} = 0$ [53] in order to clarify how the breaking of these symmetries affects the $C_V^{(3)}$.

Figures 9(a) and (b) show that $C_V^{(3)}$, W_V and Θ_V for $\alpha_{\text{dif}} = \gamma_{\text{dif}} = 0.0$ as functions of the gate voltage ξ_d for strong interaction $U/(\pi\Delta) = 5.0$ for SU(4) and SU(6) quantum dots. In the strong-coupling limit region $|\xi_d| \lesssim (N-2)U/2$, $C_V^{(3)}$ takes plateau structures of the height $(64/\pi^2)C_V^{(3)} \simeq 2.67$ for SU(4), and 2.0 for SU(6). In particular, the plateau at half filling, i.e., at $\xi_d = 0$, is caused by the two-body correlation W_V . In contrast, the

plateau around the Kondo state with the fillings of $\langle n_d \rangle \simeq 1.0$ and $N - 1$, i.e., corresponding to the one electron and one hole occupancies, are caused by the three-body correlation Θ_V . Specifically, among three independent components defined in Eqs. (2.24)–(2.26), $\tilde{\Theta}_{II}$ determines the peak structure of Θ_V since $\Theta_V \simeq -2\tilde{\Theta}_{II}$ owing to the property $\Theta_I \simeq -\Theta_{II}$ in the strongly correlated region. In the limit of $|\xi_d| \rightarrow \infty$ outside the plateau, the coefficient approaches the noninteracting value $(64/\pi^2) C_V^{(3)} \rightarrow -3$, $W_V \rightarrow -1.0$, and $\Theta_V \rightarrow -2.0$, given by Eqs. (5.3)–(5.5).

In Figs. 9(c) and (d), $C_V^{(3)}$ for $\alpha_{\text{dif}} = \gamma_{\text{dif}} = 0.0$ is plotted as a function of ξ_d , varying interaction strengths (c) $U/(\pi\Delta) = 1/3, 2/3, 5/3, 10/3, 5.0$ for SU(4), and (d) $U/(\pi\Delta) = 2/5, 1.0, 2.0, 5.0$ for SU(6). The plateau structure and the peak at the edge of the plateau of $C_V^{(3)}$ as shown above appear as U increases in the strong-coupling limit $|\xi_d| \lesssim (N - 2)U/2$.

C. Effects of tunnel asymmetries $\gamma_{\text{dif}} \neq 0$ on $C_V^{(3)}$ for symmetric bias voltages $\alpha_{\text{dif}} = 0$

We next consider the effect of tunnel asymmetry on $C_V^{(3)}$, setting bias voltages to be symmetric $\alpha_{\text{dif}} = 0$. In this case, among the three types of quadratic terms α_{dif}^2 , $\alpha_{\text{dif}}\gamma_{\text{dif}}$, and γ_{dif}^2 in Eqs. (2.21)–(2.23), the only γ_{dif}^2 term remains finite and contributes to $C_V^{(3)}$:

$$W_V \xrightarrow{\alpha_{\text{dif}}=0} -\cos 2\delta \left[1 + \left\{ \frac{5}{N-1} + \frac{3(N-2)}{N-1} \gamma_{\text{dif}}^2 \right\} \tilde{K}^2 \right], \quad (5.6)$$

$$\Theta_V \xrightarrow{\alpha_{\text{dif}}=0} \Theta_I + 3\tilde{\Theta}_{II} + 6\gamma_{\text{dif}}^2 \tilde{\Theta}_{III}. \quad (5.7)$$

The γ_{dif}^2 term emerges for $N \geq 3$. In particular, it couples to $\tilde{\Theta}_{III}$, the three-body correlation between electrons in three different levels which does not contribute to $C_V^{(3)}$ for symmetric tunnel couplings.

In the strongly correlated region for large U , the three-body part of $C_V^{(3)}$ takes a simplified form $\Theta_V \propto 1 - 3\gamma_{\text{dif}}^2$ which does not depend on α_{dif} , as shown in Eq. (5.2). Therefore, Θ_V decreases as tunnel asymmetry which enters through γ_{dif}^2 increases, and vanishes $\Theta_V \simeq 0.0$ at $\gamma_{\text{dif}} = \pm 1/\sqrt{3} (\simeq \pm 0.577)$. In particular, $\tilde{\Theta}_{II}$ has a wide plateau at the fillings $\langle n_d \rangle \simeq 1$ and $N - 1$ for large U in Fig. 2(b) and Fig. 4(b), the contribution of the three-body correlations Θ_V becomes significant at these fillings.

The NRG results of $C_V^{(3)}$, W_V , and Θ_V , for the bias symmetric case $\alpha_{\text{dif}} = 0.0$ are plotted vs ξ_d in the top, upper-middle, and lower-middle panels of Fig. 10, for (left panels) SU(4) and (right panels) SU(6) quantum dots, choosing interaction strength to be $U/(\pi\Delta) = 5.0$. Specifically, Fig. 10 (a)–(f) are obtained, varying tunnel asymmetries, as $\gamma_{\text{dif}} = 0.0, 0.2, 0.5, 0.58$ and 0.8 . The plateau of $C_V^{(3)}$ emerging at $|\xi_d| \lesssim U/2$ is due to the half-filling Kondo state $\langle n_d \rangle \simeq N/2$. The height of

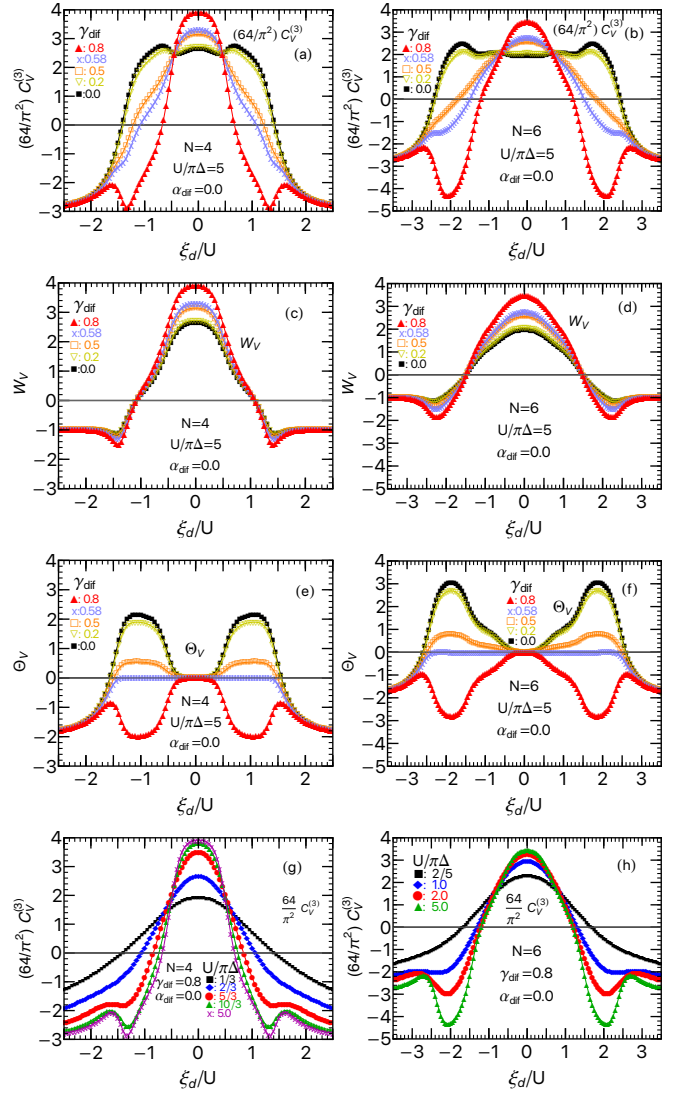


FIG. 10. Effects of tunnel asymmetry γ_{dif} on order $(eV)^3$ nonlinear current: (Top panels) $C_V^{(3)}$, and the components (Upper middle panels) W_V and (Lower middle panels) Θ_V defined in Eqs. (5.6) and (5.7) for symmetrical bias voltages $\alpha_{\text{dif}} = 0.0$ are plotted vs ξ_d/U , varying tunnel asymmetries, as for $\gamma_{\text{dif}} = 0.0$ (■), 0.2 (▽), 0.5 (□), 0.58 (×), 0.8 (△). Interaction strength is chosen to be $U/(\pi\Delta) = 5.0$ for (a)–(f): (Left panels) for SU(4) quantum dots, and (Right panels) for SU(6) quantum dots. Bottom panels: U dependence of $C_V^{(3)}$, calculated for a fixed large tunnel asymmetry $\gamma_{\text{dif}} = 0.8$, (g) $U/(\pi\Delta) = 1/3$ (■), $2/3$ (◇), $5/3$ (○), $10/3$ (△), 5.0 (×) for SU(4), and (h) $U/(\pi\Delta) = 2/5$ (■), 1.0 (◇), 2.0 (○), 5.0 (△) for SU(6).

this plateau increases with γ_{dif} , and approaches the upper bound $(64/\pi^2) C_V^{(3)} \rightarrow 4 + 2/(N - 1)$ in the limit $\gamma_{\text{dif}}^2 \rightarrow 1$. This structure is determined by the two-body part W_V as the three-body part Θ_V vanishes around the electron-hole symmetric point $\xi_d = 0$.

We see that the plateau structure of $C_V^{(3)}$ at the Kondo

states away from half filling depend sensitively on tunnel asymmetry. The positive plateau emerging at $|\xi_d| \simeq (N-2)U/2$ are due to the Kondo state of the filling $\langle n_d \rangle \simeq 1$ and $N-1$. It disappears as γ_{dif} increases, and a negative dip develops for $\gamma_{\text{dif}}^2 \geq 1/3$. This behavior of $C_V^{(3)}$ reflects the evolution of the three-body part Θ_V , which is determined by Eq. (5.2) in the strongly correlated region. Therefore, if $C_V^{(3)}$ is measured varying tunneling asymmetries γ_{dif} , the three-body correlation function Θ_V and $\tilde{\Theta}_{\text{III}}$ can experimentally be deduced, using Eqs. (5.2) and (5.7).

In the limit of $|\xi_d| \rightarrow \infty$, the coefficients approach the noninteracting value: $W_V \rightarrow -1$, $\Theta \rightarrow -2$, and $(64/\pi^2) C_V^{(3)} \rightarrow -3$ for symmetric bias $\alpha_{\text{dif}} = 0$.

Figures 10(g) and (h) compare $C_V^{(3)}$ for several different interaction strengths: (g) $U/(\pi\Delta) = 1/3, 2/3, 5/3, 10/3, 5.0$ for SU(4), and (h) $U/(\pi\Delta) = 2/5, 1.0, 2.0, 5.0$ for SU(6), choosing a large tunnel asymmetry $\gamma_{\text{dif}} = 0.8$. The dip structure due to the Kondo state at the filling $\langle n_d \rangle = 1$ and $N-1$ becomes clear as U increases, as well as the plateau due to the half-filling Kondo state.

D. $C_V^{(3)}$ under asymmetric bias voltages $\alpha_{\text{dif}} \neq 0$

The coefficient $C_V^{(3)}$ depends on the bias and tunnel asymmetries through the terms of order α_{dif}^2 , $\alpha_{\text{dif}}\gamma_{\text{dif}}$, and γ_{dif}^2 , in Eqs. (2.22) and (2.23). We have discussed in the role of the γ_{dif}^2 term of the tunnel asymmetry, setting the bias voltages to be symmetric $\alpha_{\text{dif}} = 0$. In

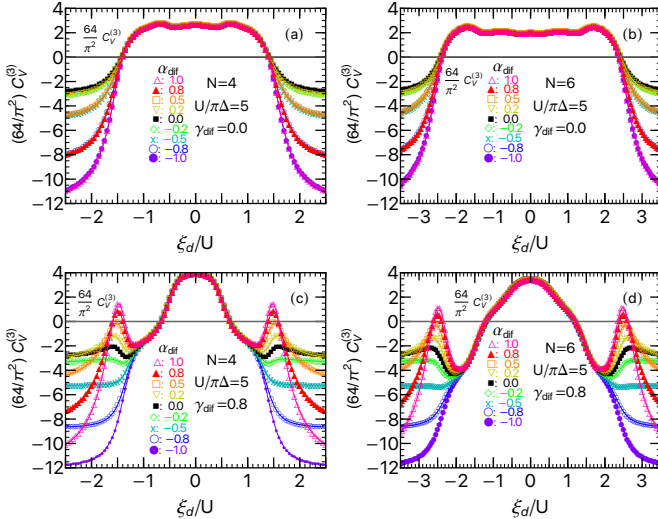


FIG. 11. Behavior of $C_V^{(3)}$ for two different tunnel couplings, (top panels) $\gamma_{\text{dif}} = 0.0$ and (bottom panels) $\gamma_{\text{dif}} = 0.8$, is plotted as a function of ξ_d , varying bias asymmetries $\alpha_{\text{dif}} = -1.0$ (\bullet), -0.8 (\circ), -0.5 (\times), -0.2 (\diamond), 0.0 (\blacksquare), 0.2 (∇), 0.5 (\square), 0.8 (\blacktriangle) and 1.0 (\triangle). Interaction strength is fixed at $U/(\pi\Delta) = 5.0$, for both (left panels) SU(4) and (right panels) SU(6) quantum dots.

this section, we examine the contributions of the other two terms, α_{dif}^2 and $\alpha_{\text{dif}}\gamma_{\text{dif}}$.

1. Effects of bias asymmetry at small $\gamma_{\text{dif}} = 0$ and large $\gamma_{\text{dif}} = 0.8$ tunnel asymmetries

In Fig. 11, the coefficient $C_V^{(3)}$ is plotted vs ξ_d , for (left panels) SU(4) and (right panels) SU(6) quantum dots, varying bias asymmetries $\alpha_{\text{dif}} = 0.0, \pm 0.2, \pm 0.5, \pm 0.8$ and ± 1.0 . Specifically, two different tunnel couplings are examined. One (top panels) is the symmetric coupling $\gamma_{\text{dif}} = 0.0$, at which the role of the α_{dif}^2 term can be clarified. The other one (bottom panels) is a large asymmetric coupling $\gamma_{\text{dif}} = 0.8$, for which all the quadratic terms, α_{dif}^2 , $\alpha_{\text{dif}}\gamma_{\text{dif}}$, and γ_{dif}^2 contribute to $C_V^{(3)}$.

As a large interaction $U/(\pi\Delta) = 5.0$ is chosen for each of the panels, the coefficient $C_V^{(3)}$ does not depend on bias asymmetry α_{dif} in the region of $|\xi_d| \lesssim (N-1)U/2$, and it takes the values determined by γ_{dif}^2 with Eqs. (5.1) and (5.2).

In contrast, the coefficient $C_V^{(3)}$ varies with $\alpha_{\text{dif}}\gamma_{\text{dif}}$ in the valence fluctuation regime $|\xi_d| \gtrsim (N-1)U/2$. It approaches the asymptotic value which is given by Eq. (5.5) in the limit of $|\xi_d| \rightarrow \infty$. Since the effect of the bias asymmetry in the tunnel symmetric case $\gamma_{\text{dif}} = 0.0$ is determined by the terms of α_{dif}^2 , the results shown in Figs. 11(a) and (b) do not vary with the sign of the parameter α_{dif} .

In Figs. 11(c) and (d), the coefficient $C_V^{(3)}$ has a sharp peak in the valence fluctuation region at $\xi_d \simeq \pm(N-1)U/2$, which grows as bias asymmetry α_{dif} increases. This is caused by the cross term with a positive sign $\alpha_{\text{dif}}\gamma_{\text{dif}} > 0$: we will examine the contributions of this term to the peak structures more precisely in the following.

2. Effects of tunnel asymmetry $\gamma_{\text{dif}} \neq 0$ on $C_V^{(3)}$ at large bias asymmetry $\alpha_{\text{dif}} = 1$

The bias and tunnel asymmetries affect the coefficient $C_V^{(3)}$ through thus quadratic terms α_{dif}^2 , $\alpha_{\text{dif}}\gamma_{\text{dif}}$, and γ_{dif}^2 in Eqs. (2.21)–(2.23). In order to clarify the contribution of the cross term, we set the bias asymmetry to be the upper-bound value $\alpha_{\text{dif}} = 1$, which describes the situation where the bias asymmetry is maximized by grounding the right leads. Therefore, in this case W_V and Θ_V can be expressed in the following form,

$$W_V \xrightarrow{\alpha_{\text{dif}}=1} -\cos 2\delta \left[4 - 6(1 + \gamma_{\text{dif}}) \tilde{K} + \left\{ \frac{3N+2}{N-1} + 6\gamma_{\text{dif}} + \frac{3(N-2)}{N-1} \gamma_{\text{dif}}^2 \right\} \tilde{K}^2 \right], \quad (5.8)$$

$$\Theta_V \xrightarrow{\alpha_{\text{dif}}=1} 4 \left[\Theta_I + 6 \left(\frac{1 + \gamma_{\text{dif}}}{2} \right) \tilde{\Theta}_{\text{II}} + 6 \left(\frac{1 - \gamma_{\text{dif}}}{2} \right) \tilde{\Theta}_{\text{III}} \right]. \quad (5.9)$$

Here, the cross term $\alpha_{\text{dif}}\gamma_{\text{dif}}$ appears as linear order terms with respect to γ_{dif} .

Our discussion here is based on Fig. 12, in which the NRG results of $C_V^{(3)}$ for SU(4) quantum dots and those for SU(6) quantum dots are presented in the left and

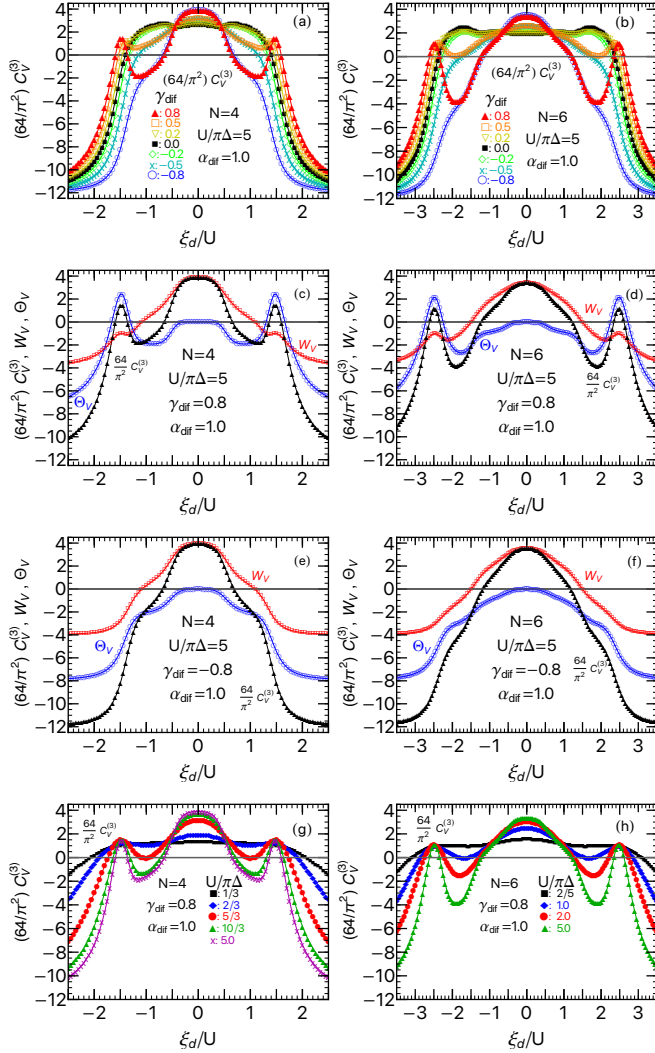


FIG. 12. Behavior of $C_V^{(3)}$ at large bias asymmetry $\alpha_{\text{dif}} = 1$ is plotted vs ξ_d for (left panels) SU(4) and (right panels) SU(6) quantum dots. Top panels: tunnel asymmetry is varied, as $\gamma_{\text{dif}} = -0.8$ (\circ), -0.5 (\times), -0.2 (\diamond), 0.0 (\blacksquare), 0.2 (∇), 0.5 (\square), 0.8 (\triangle). In addition, two-body part W_V (\square) and three-body part Θ_V (\circ) are plotted together with $C_V^{(3)}$ (\blacktriangle) for two large opposite tunnel asymmetries: (upper middle panels) $\gamma_{\text{dif}} = 0.8$, and (lower middle panels) $\gamma_{\text{dif}} = -0.8$. Interaction strength is chosen to be $U/(\pi\Delta) = 5.0$ in (a)–(f). Bottom panels show the U dependence of $C_V^{(3)}$ for $\gamma_{\text{dif}} = 0.8$: (g) $U/(\pi\Delta) = 1/3, 2/3, 5/3, 10/3, 5.0$ for SU(4), and (h) $U/(\pi\Delta) = 2/5, 1.0, 2.0, 5.0$ for SU(6).

right panels, respectively. Top panels of Fig. 12 show $C_V^{(3)}$ as a function of the gate voltage ξ_d , varying tunneling asymmetries $\gamma_{\text{dif}} = 0.0, \pm 0.2, \pm 0.5, \pm 0.8$, for a strong interaction strength $U/(\pi\Delta) = 5.0$. The upper middle panels show $C_V^{(3)}, W_V, \Theta_V$ for large positive tunnel asymmetries $\gamma_{\text{dif}} = 0.8$, and correspondingly lower middle panels show the ones for large negative tunnel asymmetries $\gamma_{\text{dif}} = -0.8$. Bottom panels of Fig. 12 show the results, calculated for several interaction strengths $U/(\pi\Delta) = 1/3, 2/3, 5/3, 10/3, 5.0$ for SU(4), and $U/(\pi\Delta) = 2/5, 1.0, 2.0, 5.0$ for SU(6), taking asymmetric tunnel coupling to be $\gamma_{\text{dif}} = 0.8$.

In the strongly correlated region $|\xi_d| \lesssim (N-1)U/2$ for large U , the result of $C_V^{(3)}$ in Figs. 12 (a) and (b) almost does not depend on whether or not $\alpha_{\text{dif}} = 1$, and the behavior in this region is determined essentially by the γ_{dif}^2 term in Eqs. (5.1) and (5.2). The cross term $\alpha_{\text{dif}}\gamma_{\text{dif}}$ becomes important at $|\xi_d| \gtrsim (N-1)U/2$, outside the correlated region.

In particular, $C_V^{(3)}$ takes a sharp peak near $\xi_d \simeq (N-1)U/2$ in the valence fluctuation regime for large positive γ_{dif} , i.e., $\alpha_{\text{dif}}\gamma_{\text{dif}} > 0$ at which bias and tunneling asymmetries cooperatively enhance the charge transfer from one of the electrodes. The results of W_V and Θ_V , plotted for $\gamma_{\text{dif}} = 0.8$ in Fig. 12 (c)–(d), show the sharp peak structure is mainly due to the three-body part Θ_V and two-body part has a small constructive peak at the same position. In contrast, for tunnel asymmetry in the opposite direction $\gamma_{\text{dif}} = -0.8$, each of the two components, W_V and Θ_V , does not have a peak in Fig. 12 (e)–(f).

We consider more precisely the peak that emerged in the three-body part Θ_V , taking the limit of $\gamma_{\text{dif}} \rightarrow 1$ in Eq. (5.9) [70],

$$\Theta_V \xrightarrow{\alpha_{\text{dif}}=1, \gamma_{\text{dif}} \rightarrow 1} 4 \left(\Theta_I + 6 \tilde{\Theta}_{\text{II}} + 6 \tilde{\Theta}_{\text{III}} \right). \quad (5.10)$$

Note that each of the three-body correlation functions of the SU(N) symmetric quantum dots has a definite sign: $\Theta_I < 0$, $\tilde{\Theta}_{\text{II}} > 0$, and $\tilde{\Theta}_{\text{III}} < 0$, as shown in Figs. 2 and 4. Specifically, in the valence fluctuation regime, the positive contribution of $6 \tilde{\Theta}_{\text{II}}$ in Eq. (5.10) becomes greater than the negative contribution of $\Theta_I + 6 \tilde{\Theta}_{\text{III}}$, and the difference between these components yields a sharp peak of Θ_V at $|\xi_d| \gtrsim (N-1)U/2$. The height increase measured from the base value of Θ_V , which can be defined at the Kondo state in the close vicinity of the valence fluctuation region, increases with N . Note that in the Kondo state, the three-body correlation functions have a property $\tilde{\Theta}_I \simeq -\tilde{\Theta}_{\text{II}} \simeq \tilde{\Theta}_{\text{III}}$, and Θ_V in this limit $\gamma_{\text{dif}} \rightarrow 1$ takes a negative value $\Theta_V \rightarrow 4\Theta_I < 0$. In the opposite limit of the tunnel asymmetries $\gamma_{\text{dif}} \rightarrow -1$, the cross term is negative $\alpha_{\text{dif}}\gamma_{\text{dif}} < 0$. Therefore, the three-body contribution also becomes negative $\Theta_V \rightarrow 4\Theta_I < 0$, and $C_V^{(3)}$ monotonically decreases at $|\xi_d| \gtrsim (N-1)U/2$.

We also examine how the peak structure evolves with U in Figs. 12(g) and (h). The results show that the

dip structure in the $SU(N)$ Kondo regime near $|\xi_d| \simeq (N-1)U/2$ and the sharp peak structure in the valence fluctuation regime $|\xi_d| \gtrsim (N-1)U/2$ clearer as interaction U increases.

VI. CONCLUSION

We have derived the exact low-bias expansion formula of the differential conductance dI/dV through a multilevel Anderson impurity up to terms of order $(eV)^2$, without assuming symmetries in tunnel couplings or bias voltages. It is applicable to a wide class of quantum dots with arbitrary energy level $\epsilon_{d\sigma}$. The expansion coefficients are expressed in terms of the phase shift δ_σ , linear susceptibilities $\chi_{\sigma\sigma'}$, and three-body correlation functions $\chi_{\sigma\sigma'\sigma''}^{[3]}$, defined with respect to the equilibrium ground state.

The tunnel and bias asymmetries enter the transport coefficients through the parameters $\gamma_{\text{dif}} = (\Gamma_L - \Gamma_R)/(\Gamma_L + \Gamma_R)$ and $\alpha_{\text{dif}} = (\mu_L + \mu_R - 2E_F)/(\mu_L - \mu_R)$. In contrast to the linear conductance which depends only on the tunnel asymmetry through the prefactor $g_0 = (e^2/h)4\Gamma_L\Gamma_R/(\Gamma_L + \Gamma_R)^2$, the nonlinear terms $c_{V,\sigma}^{(2)}$ and $c_{V,\sigma}^{(3)}$, given in Eqs. (B.5) and (B.6), depend on both asymmetries. The γ_{dif} -dependence enters additionally through the self-energy corrections due to the Coulomb interactions, and the α_{dif} -dependence arises also through a shift of bias window. In particular, $c_{V,\sigma}^{(2)}$ emerges when tunnel couplings and/or bias voltages are asymmetrical, and is given by a linear combination of γ_{dif} and α_{dif} .

We have explored the behaviors of these coefficients of $SU(N)$ quantum dots of $N = 4$ and 6 with the NRG, in a wide range of parameter space, the varying gate voltage ξ_d and interaction U as well as γ_{dif} and α_{dif} . In particular, for large U , transport exhibits quite different behaviors depending on electron fillings, especially in the two regions: one is the strongly-correlated region $1 \lesssim \langle n_d \rangle \lesssim N-1$, and the other is the valence fluctuation region in which $0 \lesssim \langle n_d \rangle \lesssim 1$ or $N-1 \lesssim \langle n_d \rangle \lesssim N$. The coefficient $C_V^{(2)}$ of the first nonlinear term of dI/dV for $SU(N)$ quantum dots becomes almost independent of bias asymmetries in the strongly-correlated region as charge fluctuation is suppressed in this region. Conversely, it becomes less sensitive to tunnel asymmetries in the valence fluctuation region since interaction effects are suppressed as the filling approaches $\langle n_d \rangle \rightarrow 0$ or N .

The three-body correlation functions contribute to the order $(eV)^2$ nonlinear term of dI/dV , especially in the $SU(N)$ Kondo regime other than the half-filled one occurring in electron-hole asymmetric cases, and also in the valence fluctuation region. The coefficient $C_V^{(3)}$ of the order $(eV)^2$ term shows the quadratic α_{dif}^2 , $\alpha_{\text{dif}}\gamma_{\text{dif}}$ and γ_{dif}^2 dependences on the bias and tunnel asymmetries.

In particular, the γ_{dif}^2 term, which is absent in the $SU(2)$ case, emerges for multilevel quantum dots with

$N \geq 3$, and it couples to a three-body correlation between electrons occupying three different local levels: $\chi_{\sigma\sigma'\sigma''}^{[3]}$ for $\sigma \neq \sigma' \neq \sigma'' \neq \sigma$. We have found that, as γ_{dif}^2 increases, the structure of $SU(N)$ Kondo plateaus of $C_V^{(3)}$ at $\langle n_d \rangle \simeq 1$ and $N-1$ fillings vary significantly from the one for symmetric junctions with $\gamma_{\text{dif}} = \alpha_{\text{dif}} = 0$. It suggests that the tunnel asymmetries could be used as a sensitive probe for observing three-body correlations in the $SU(N)$ Kondo states.

The cross term $\alpha_{\text{dif}}\gamma_{\text{dif}}$ plays an important role, especially in the valence fluctuation region. It yields a sharp peak of $C_V^{(3)}$ when $\alpha_{\text{dif}}\gamma_{\text{dif}} > 0$, i.e., in the case at which the tunneling and bias asymmetries cooperatively enhance the charge transfer from one of the electrodes. This is caused by a constructive enhancement of the three-independent components of the three-body correlation function of $SU(N)$ quantum dots: $\chi_{\sigma\sigma\sigma}^{[3]}$, $\chi_{\sigma\sigma'\sigma'}^{[3]}$, and $\chi_{\sigma\sigma'\sigma''}^{[3]}$. Our results indicate that these three-independent components can separately be deduced if $C_V^{(3)}$ is measured varying tunneling asymmetries γ_{dif} and bias asymmetries α_{dif} .

ACKNOWLEDGMENTS

This work was supported by JSPS KAKENHI Grant Nos. JP18K03495, JP18J10205, JP21K03415, and JP23K03284, and by JST CREST Grant No. JPMJCR1876. KM was supported by JST, the establishment of university fellowships towards the creation of science technology innovation, Grant Number JPMJFS2138.

Appendix A: Fermi-liquid relations

The retarded Green's function defined in Eq. (2.9) can be expressed in the form,

$$G_\sigma^r(\omega) = \frac{1}{\omega - \epsilon_{d\sigma} + i\Delta - \Sigma_\sigma^r(\omega)}. \quad (\text{A1})$$

Specifically, the ground-state properties and the leading Fermi-liquid corrections are determined by the low-frequency behavior of the equilibrium self-energy $\Sigma_{\text{eq},\sigma}^r(\omega) \equiv \Sigma_\sigma^r(\omega)|_{T=eV=0}$, or the Green's function:

$$G_\sigma^r(\omega) \simeq \frac{z_\sigma}{\omega - \tilde{\epsilon}_{d\sigma} + i\tilde{\Delta}_\sigma}. \quad (\text{A2})$$

Here, the renormalized parameters are defined by

$$\begin{aligned} \tilde{\epsilon}_{d\sigma} &\equiv z_\sigma [\epsilon_{d\sigma} + \Sigma_{\text{eq},\sigma}^r(0)] = \tilde{\Delta}_\sigma \cot \delta_\sigma, \\ \tilde{\Delta}_\sigma &\equiv z_\sigma \Delta, \quad \frac{1}{z_\sigma} \equiv 1 - \left. \frac{\partial \Sigma_{\text{eq},\sigma}^r(\omega)}{\partial \omega} \right|_{\omega=0}. \end{aligned} \quad (\text{A3})$$

Furthermore, the renormalization factor z_σ and the derivative of $\Sigma_{\text{eq},\sigma}^r(0)$ with respect to the impurity level

$\epsilon_{d\sigma'}$ are related to each other through the Ward identity [4, 7]:

$$\frac{1}{z_\sigma} = \tilde{\chi}_{\sigma\sigma}, \quad \tilde{\chi}_{\sigma\sigma'} \equiv \delta_{\sigma\sigma'} + \frac{\partial \Sigma_{\text{eq},\sigma}^r(0)}{\partial \epsilon_{d\sigma'}}. \quad (\text{A4})$$

Note that $\tilde{\chi}_{\sigma\sigma'}$ corresponds to an enhancement factor for the linear susceptibilities defined in Eq. (2.7), i.e., $\chi_{\sigma\sigma'} = -\partial \langle n_{d\sigma} \rangle / \partial \epsilon_{d\sigma'} = \rho_{d\sigma} \tilde{\chi}_{\sigma\sigma'}$ at $T = 0$.

Recently, the Ward identity for the order ω^2 real part of the self-energy has also been obtained, as [50–53]

$$\frac{\partial^2}{\partial \omega^2} \text{Re} \Sigma_{\text{eq},\sigma}^r(\omega) \Big|_{\omega \rightarrow 0} = \frac{\partial^2 \Sigma_{\text{eq},\sigma}^r(0)}{\partial \epsilon_{d\sigma}^2} = \frac{\partial \tilde{\chi}_{\sigma\sigma}}{\partial \epsilon_{d\sigma}}. \quad (\text{A5})$$

This identity shows that the ω^2 real part is determined by the intra-level component of the three-body correlation function $\chi_{\sigma\sigma\sigma}^{[3]}$. Physically, this term of the self-energy induces higher-order energy shifts for single-quasiparticle excitations.

Appendix B: Derivation of $c_{V,\sigma}^{(2)}$ and $c_{V,\sigma}^{(3)}$

We describe here the derivation of the coefficients $c_{V,\sigma}^{(2)}$ and $c_{V,\sigma}^{(3)}$ which appeared in Eq. (1.1). The low-energy asymptotic form of the retarded self-energy $\Sigma_\sigma^r(\omega)$ for multi-orbital Anderson impurity model was derived up to terms of order ω^2 , T^2 , and $(eV)^2$ in previous work

[53, 63],

$$\begin{aligned} \text{Im} \Sigma_\sigma^r(\omega) &= -\frac{\pi}{2} \frac{1}{\rho_{d\sigma}} \sum_{\sigma'(\neq\sigma)} \chi_{\sigma\sigma'}^2 \\ &\times \left[(\omega - \alpha eV)^2 + \frac{3\Gamma_L \Gamma_R}{(\Gamma_L + \Gamma_R)^2} (eV)^2 + (\pi T)^2 \right] + \dots, \end{aligned} \quad (\text{B1})$$

$$\begin{aligned} \text{Re} \Sigma_\sigma^r(\omega) &= \Sigma_{\text{eq},\sigma}^r(0) - \sum_{\sigma'(\neq\sigma)} \tilde{\chi}_{\sigma\sigma'} \alpha eV + (1 - \tilde{\chi}_{\sigma\sigma}) \omega \\ &+ \frac{1}{6} \frac{1}{\rho_{d\sigma}} \sum_{\sigma'(\neq\sigma)} \frac{\partial \chi_{\sigma\sigma'}}{\partial \epsilon_{d\sigma'}} \left[\frac{3\Gamma_L \Gamma_R}{(\Gamma_L + \Gamma_R)^2} (eV)^2 + (\pi T)^2 \right] \\ &+ \frac{1}{2} \frac{\partial \tilde{\chi}_{\sigma\sigma}}{\partial \epsilon_{d\sigma}} \omega^2 + \sum_{\sigma'(\neq\sigma)} \frac{\partial \tilde{\chi}_{\sigma\sigma'}}{\partial \epsilon_{d\sigma}} \alpha eV \omega \\ &+ \frac{1}{2} \sum_{\sigma'(\neq\sigma)} \sum_{\sigma''(\neq\sigma)} \frac{\partial \tilde{\chi}_{\sigma\sigma'}}{\partial \epsilon_{d\sigma''}} \alpha^2 (eV)^2 + \dots. \end{aligned} \quad (\text{B2})$$

Here, α is a parameter defined in a way such that $\alpha eV \equiv (\Gamma_L \mu_L + \Gamma_R \mu_R) / (\Gamma_L + \Gamma_R)$, and thus

$$\alpha \equiv \frac{\alpha_L \Gamma_L - \alpha_R \Gamma_R}{\Gamma_L + \Gamma_R} = \frac{1}{2} (\alpha_{\text{dif}} + \gamma_{\text{dif}}). \quad (\text{B3})$$

The spectral function can be deduced exactly up to terms of order ω^2 , T^2 , and $(eV)^2$ from the above results of $\Sigma_\sigma^r(\omega)$ using Eq. (A1):

$$\begin{aligned} \pi \Delta A_\sigma(\omega) &= \sin^2 \delta_\sigma + \pi \sin 2\delta_\sigma \left[\chi_{\sigma\sigma} \omega + \sum_{\sigma'(\neq\sigma)} \chi_{\sigma\sigma'} \frac{1}{2} (\alpha_{\text{dif}} + \gamma_{\text{dif}}) eV \right] \\ &+ \pi^2 \left[\cos 2\delta_\sigma \left(\chi_{\sigma\sigma}^2 + \frac{1}{2} \sum_{\sigma'(\neq\sigma)} \chi_{\sigma\sigma'}^2 \right) - \frac{\sin 2\delta_\sigma}{2\pi} \chi_{\sigma\sigma\sigma}^{[3]} \right] \omega^2 \\ &+ \pi^2 \left[\cos 2\delta_\sigma \sum_{\sigma'(\neq\sigma)} \left(\chi_{\sigma\sigma} \chi_{\sigma\sigma'} - \frac{1}{2} \chi_{\sigma\sigma'}^2 \right) - \frac{\sin 2\delta_\sigma}{2\pi} \sum_{\sigma'(\neq\sigma)} \chi_{\sigma\sigma\sigma'}^{[3]} \right] (\alpha_{\text{dif}} + \gamma_{\text{dif}}) \omega eV \\ &+ \frac{\pi^2}{3} \sum_{\sigma'(\neq\sigma)} \left[\frac{3}{2} \cos 2\delta_\sigma \chi_{\sigma\sigma'}^2 - \frac{\sin 2\delta_\sigma}{2\pi} \chi_{\sigma\sigma'\sigma'}^{[3]} \right] \left[\frac{3}{4} \left(1 + 2\alpha_{\text{dif}} \gamma_{\text{dif}} + \alpha_{\text{dif}}^2 \right) (eV)^2 + (\pi T)^2 \right] \\ &+ \frac{\pi^2}{3} \sum_{\sigma'(\neq\sigma)} \sum_{\sigma''(\neq\sigma,\sigma')} \left[\cos 2\delta_\sigma \chi_{\sigma\sigma'} \chi_{\sigma\sigma''} - \frac{\sin 2\delta_\sigma}{2\pi} \chi_{\sigma\sigma'\sigma''}^{[3]} \right] \frac{3}{4} \left(\gamma_{\text{dif}}^2 + 2\alpha_{\text{dif}} \gamma_{\text{dif}} + \alpha_{\text{dif}}^2 \right) (eV)^2 + \dots. \end{aligned} \quad (\text{B4})$$

Substituting this low-energy asymptotic form into the the Landauer-type formula in Eq. (2.13), we obtain the

exact expression for the coefficients $c_{V,\sigma}^{(2)}$ and $c_{V,\sigma}^{(3)}$ for the differential conductance at $T = 0$ defined in Eq. (1.1):

$$c_{V,\sigma}^{(2)} = \pi \sin 2\delta_\sigma \left[\alpha_{\text{dif}} \chi_{\sigma\sigma} + (\alpha_{\text{dif}} + \gamma_{\text{dif}}) \sum_{\sigma'(\neq\sigma)} \chi_{\sigma\sigma'} \right], \quad (\text{B5})$$

$$c_{V,\sigma}^{(3)} = \frac{\pi^2}{4} \left[-\cos 2\delta_\sigma \left\{ (1 + 3\alpha_{\text{dif}}^2) \chi_{\sigma\sigma}^2 + (5 - 3\gamma_{\text{dif}}^2) \sum_{\sigma'(\neq\sigma)} \chi_{\sigma\sigma'}^2 + 6\alpha_{\text{dif}} (\alpha_{\text{dif}} + \gamma_{\text{dif}}) \chi_{\sigma\sigma} \sum_{\sigma'(\neq\sigma)} \chi_{\sigma\sigma'} \right. \right. \\ \left. \left. + 3(\alpha_{\text{dif}} + \gamma_{\text{dif}})^2 \sum_{\sigma'(\neq\sigma)} \sum_{\sigma''(\neq\sigma)} \chi_{\sigma\sigma'} \chi_{\sigma\sigma''} \right\} \right. \\ \left. + \frac{\sin 2\delta_\sigma}{2\pi} \left\{ (1 + 3\alpha_{\text{dif}}^2) \chi_{\sigma\sigma\sigma}^{[3]} + 6\alpha_{\text{dif}} (\alpha_{\text{dif}} + \gamma_{\text{dif}}) \sum_{\sigma'(\neq\sigma)} \chi_{\sigma\sigma\sigma'}^{[3]} + 3(1 - \gamma_{\text{dif}}^2) \sum_{\sigma'(\neq\sigma)} \chi_{\sigma\sigma'\sigma'}^{[3]} \right. \right. \\ \left. \left. + 3(\alpha_{\text{dif}} + \gamma_{\text{dif}})^2 \sum_{\sigma'(\neq\sigma)} \sum_{\sigma''(\neq\sigma)} \chi_{\sigma\sigma'\sigma''}^{[3]} \right\} \right]. \quad (\text{B6})$$

Note that $c_{V,\sigma}^{(2)}$ is proportional to the derivative of the density of state as $\sin 2\delta_\sigma = \Delta\rho'_{d\sigma}/\chi_{\sigma\sigma}$ from Eq. (2.12). The coefficients $c_{V,\sigma}^{(2)}$ and $c_{V,\sigma}^{(3)}$ have odd and even inversion-symmetrical properties, respectively. Namely, if the left and right leads are inverted together with their tunnel couplings and chemical potentials, sign of $c_{V,\sigma}^{(2)}$ changes while $c_{V,\sigma}^{(3)}$ does not:

$$c_{V,\sigma}^{(2)}(\alpha_{\text{dif}}, \gamma_{\text{dif}}) = -c_{V,\sigma}^{(2)}(-\alpha_{\text{dif}}, -\gamma_{\text{dif}}), \quad (\text{B7})$$

$$c_{V,\sigma}^{(3)}(\alpha_{\text{dif}}, \gamma_{\text{dif}}) = c_{V,\sigma}^{(3)}(-\alpha_{\text{dif}}, -\gamma_{\text{dif}}). \quad (\text{B8})$$

Appendix C: Behavior of three-body correlation functions for large U

In the $SU(N)$ symmetric case, the two different off-diagonal components $\chi_{\sigma\sigma'\sigma'}$ and $\chi_{\sigma\sigma'\sigma''}$, of the three-body correlation functions for $\sigma \neq \sigma' \neq \sigma'' \neq \sigma$ can be expressed as a linear combination of the diagonal one $\chi_{\sigma\sigma\sigma}^{[3]}$ and the derivative of the linear susceptibilities [44]:

$$(N-1)\chi_{\sigma\sigma'\sigma'}^{[3]} = -\chi_{\sigma\sigma\sigma}^{[3]} + \frac{\partial\chi_{\sigma\sigma}}{\partial\epsilon_d}, \quad (\text{C1})$$

$$\frac{(N-1)(N-2)}{2}\chi_{\sigma\sigma'\sigma''}^{[3]} = \chi_{\sigma\sigma\sigma}^{[3]} - \frac{\partial\chi_{\sigma\sigma}}{\partial\epsilon_d} + \frac{N-1}{2}\frac{\partial\chi_{\sigma\sigma'}}{\partial\epsilon_d}. \quad (\text{C2})$$

Figure 13 compares the components emerging on the right-hand side for $N=4$, i.e., $\chi_{\sigma\sigma\sigma}^{[3]}$, $\frac{\partial\chi_{\sigma\sigma}}{\partial\epsilon_d}$, and $(N-1)\frac{\partial\chi_{\sigma\sigma'}}{\partial\epsilon_d}$, varying interaction strength U . We can see that the diagonal component $|\chi_{\sigma\sigma\sigma}^{[3]}|$ becomes much larger than

the derivative terms $|\frac{\partial\chi_{\sigma\sigma}}{\partial\epsilon_d}|$ and $(N-1)|\frac{\partial\chi_{\sigma\sigma'}}{\partial\epsilon_d}|$, for strong interactions $U/(\pi\Delta) \gtrsim 2.0$, over a wide parameter range $-(N-1)U/2 \lesssim \xi_d \lesssim (N-1)U/2$. Therefore, $\chi_{\sigma\sigma\sigma}^{[3]}$ dominates on the right hand side of Eq. (C1) and also on Eq. (C2), and thus the corresponding dimensionless parameters show the property $\Theta_{\text{I}} \simeq -\Theta_{\text{II}} \simeq \tilde{\Theta}_{\text{III}}$ described in Eq. (3.1) for the strong interaction region. We have confirmed that the same behavior occurs in the $SU(6)$ symmetric case.

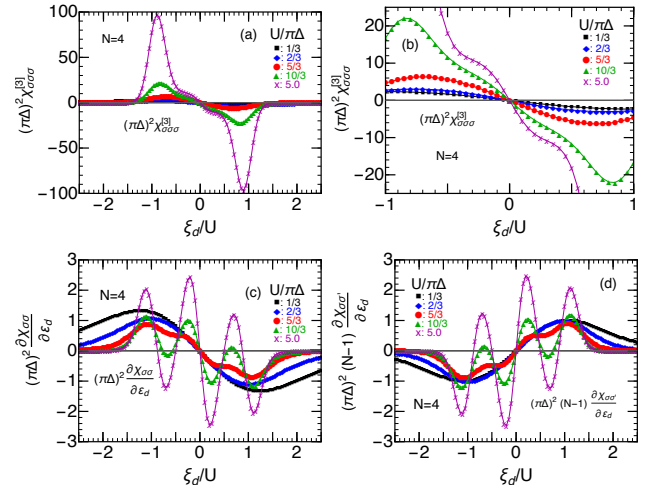


FIG. 13. Correlation functions emerging on the right-hand side of Eqs. (C1) and (C2) are plotted vs ξ_d/U , for $N=4$. (a)–(b): the diagonal component $(\pi\Delta)^2\chi_{\sigma\sigma\sigma}^{[3]}$. (c): $(\pi\Delta)^2\frac{\partial\chi_{\sigma\sigma}}{\partial\epsilon_d}$. (d): $(\pi\Delta)^2(N-1)\frac{\partial\chi_{\sigma\sigma'}}{\partial\epsilon_d}$. (b) represents an enlarged view of (a). In each of these panels, interaction strength is chosen to be $U/(\pi\Delta) = 1/3, 2/3, 5/3, 10/3, 5.0$.

[1] J. Kondo, *The Physics of Dilute Magnetic Alloys*, edited by S. Koikegami, K. Odagiri, K. Yamaji, and T. Yanag-

isawa (Cambridge University Press, 2012).

- [2] A. C. Hewson, *The Kondo Problem to Heavy Fermions* (Cambridge University Press, Cambridge, U.K., 1993).
- [3] P. Nozières, *J. Low Temp. Phys.* **17**, 31 (1974).
- [4] K. Yamada, *Prog. Theor. Phys.* **53**, 970 (1975).
- [5] K. Yamada, *Prog. Theor. Phys.* **54**, 316 (1975).
- [6] H. Shiba, *Prog. Theor. Phys.* **54**, 967 (1975).
- [7] A. Yoshimori, *Prog. Theor. Phys.* **55**, 67 (1976).
- [8] K. G. Wilson, *Rev. Mod. Phys.* **47**, 773 (1975).
- [9] H. R. Krishna-murthy, J. W. Wilkins, and K. G. Wilson, *Phys. Rev. B* **21**, 1003 (1980).
- [10] H. R. Krishna-murthy, J. W. Wilkins, and K. G. Wilson, *Phys. Rev. B* **21**, 1044 (1980).
- [11] D. Goldhaber-Gordon, H. Shtrikman, D. Mahalu, D. Abusch-Magder, U. Meirav, and M. A. Kastner, *Nature* **391**, 156 (1998).
- [12] D. Goldhaber-Gordon, J. Göres, M. A. Kastner, H. Shtrikman, D. Mahalu, and U. Meirav, *Phys. Rev. Lett.* **81**, 5225 (1998).
- [13] S. M. Cronenwett, T. H. Oosterkamp, and L. P. Kouwenhoven, *Science* **281**, 540 (1998).
- [14] W. G. van der Wiel, S. D. Franceschi, T. Fujisawa, J. M. Elzerman, S. Tarucha, and L. P. Kouwenhoven, *Science* **289**, 2105 (2000).
- [15] J. Schmid, J. Weis, K. Eberl, and K. v. Klitzing, *Physica B: Condens. Matter* **256-258**, 182 (1998).
- [16] F. Simmel, R. H. Blick, J. P. Kotthaus, W. Wegscheider, and M. Bichler, *Phys. Rev. Lett.* **83**, 804 (1999).
- [17] S. Sasaki, S. Amaha, N. Asakawa, M. Eto, and S. Tarucha, *Phys. Rev. Lett.* **93**, 017205 (2004).
- [18] M. Grobis, I. G. Rau, R. M. Potok, H. Shtrikman, and D. Goldhaber-Gordon, *Phys. Rev. Lett.* **100**, 246601 (2008).
- [19] G. D. Scott, Z. K. Keane, J. W. Ciszek, J. M. Tour, and D. Natelson, *Phys. Rev. B* **79**, 165413 (2009).
- [20] O. Zarchin, M. Zaffalon, M. Heiblum, D. Mahalu, and V. Umansky, *Phys. Rev. B* **77**, 241303(R) (2008).
- [21] T. Delattre, C. Feuillet-Palma, L. G. Herrmann, P. Morfin, J.-M. Berroir, G. Fève, B. Plaçaïs, D. C. Glatthli, M.-S. Choi, C. Mora, and T. Kontos, *Nat. Phys.* **5**, 208 (2009).
- [22] Y. Yamauchi, K. Sekiguchi, K. Chida, T. Arakawa, S. Nakamura, K. Kobayashi, T. Ono, T. Fujii, and R. Sakano, *Phys. Rev. Lett.* **106**, 176601 (2011).
- [23] I. V. Borzenets, J. Shim, J. C. H. Chen, A. Ludwig, A. D. Wieck, S. Tarucha, H.-S. Sim, and M. Yamamoto, *Nature* **579**, 210 (2020).
- [24] W. Izumida, O. Sakai, and S. Suzuki, *Journal of the Physical Society of Japan* **70**, 1045 (2001).
- [25] A. Oguri, *Phys. Rev. B* **64**, 153305 (2001).
- [26] F. B. Anders, *Phys. Rev. Lett.* **101**, 066804 (2008).
- [27] A. Weichselbaum and J. von Delft, *Phys. Rev. Lett.* **99**, 076402 (2007).
- [28] E. A. Laird, F. Kuemmeth, G. A. Steele, K. Grove-Rasmussen, J. Nygård, K. Flensberg, and L. P. Kouwenhoven, *Rev. Mod. Phys.* **87**, 703 (2015).
- [29] L. Borda, G. Zaránd, W. Hofstetter, B. I. Halperin, and J. von Delft, *Phys. Rev. Lett.* **90**, 026602 (2003).
- [30] W. Izumida, O. Sakai, and Y. Shimizu, *J. Phys. Soc. Japan* **67**, 2444 (1998).
- [31] S. Sasaki, S. De Franceschi, J. M. Elzerman, W. G. van der Wiel, M. Eto, S. Tarucha, and L. P. Kouwenhoven, *Nature* **405**, 764 (2000).
- [32] P. Jarillo-Herrero, J. Kong, H. S. J. van der Zant, C. Dekker, L. P. Kouwenhoven, and S. De Franceschi, *Phys. Rev. Lett.* **94**, 156802 (2005).
- [33] M.-S. Choi, R. López, and R. Aguado, *Phys. Rev. Lett.* **95**, 067204 (2005).
- [34] M. Eto, *Journal of the Physical Society of Japan* **74**, 95 (2005).
- [35] R. Sakano and N. Kawakami, *Phys. Rev. B* **73**, 155332 (2006).
- [36] R. Sakano, T. Kita, and N. Kawakami, *Journal of the Physical Society of Japan* **76**, 074709 (2007).
- [37] A. Makarovski, A. Zhukov, J. Liu, and G. Finkelstein, *Phys. Rev. B* **75**, 241407 (2007).
- [38] F. B. Anders, D. E. Logan, M. R. Galpin, and G. Finkelstein, *Phys. Rev. Lett.* **100**, 086809 (2008).
- [39] I. Weymann, R. Chirla, P. Trocha, and C. P. Moca, *Phys. Rev. B* **97**, 085404 (2018).
- [40] C. Mora, P. Vitushinsky, X. Leyronas, A. A. Clerk, and K. Le Hur, *Phys. Rev. B* **80**, 155322 (2009).
- [41] C. Mora, *Phys. Rev. B* **80**, 125304 (2009).
- [42] J. P. Cleuziou, N. V. N'Guyen, S. Florens, and W. Wernsdorfer, *Phys. Rev. Lett.* **111**, 136803 (2013).
- [43] D. Mantelli, C. P. Moca, G. Zaránd, and M. Grifoni, *Physica E* **77**, 180 (2016).
- [44] Y. Teratani, R. Sakano, and A. Oguri, *Phys. Rev. Lett.* **125**, 216801 (2020).
- [45] Y. Teratani, R. Sakano, R. Fujiwara, T. Hata, T. Arakawa, M. Ferrier, K. Kobayashi, and A. Oguri, *J. Phys. Soc. Japan* **85**, 094718 (2016).
- [46] M. Ferrier, T. Arakawa, T. Hata, R. Fujiwara, R. Delagrangé, R. Weil, R. Deblock, R. Sakano, A. Oguri, and K. Kobayashi, *Nat. Phys.* **12**, 230 (2016).
- [47] M. Ferrier, T. Arakawa, T. Hata, R. Fujiwara, R. Delagrangé, R. Deblock, Y. Teratani, R. Sakano, A. Oguri, and K. Kobayashi, *Phys. Rev. Lett.* **118**, 196803 (2017).
- [48] Y. Teratani, R. Sakano, T. Hata, T. Arakawa, M. Ferrier, K. Kobayashi, and A. Oguri, *Phys. Rev. B* **102**, 165106 (2020).
- [49] C. Mora, C. P. Moca, J. von Delft, and G. Zaránd, *Phys. Rev. B* **92**, 075120 (2015).
- [50] M. Filippone, C. P. Moca, A. Weichselbaum, J. von Delft, and C. Mora, *Phys. Rev. B* **98**, 075404 (2018).
- [51] A. Oguri and A. C. Hewson, *Phys. Rev. Lett.* **120**, 126802 (2018).
- [52] A. Oguri and A. C. Hewson, *Phys. Rev. B* **97**, 045406 (2018).
- [53] A. Oguri and A. C. Hewson, *Phys. Rev. B* **97**, 035435 (2018).
- [54] T. Hata, Y. Teratani, T. Arakawa, S. Lee, M. Ferrier, R. Deblock, R. Sakano, A. Oguri, and K. Kobayashi, *Nature Communications* **12**, 3233 (2021).
- [55] K. Tsutsumi, Y. Teratani, A. Oguri, and R. Sakano, in *Proceedings of the International Conference on Strongly Correlated Electron Systems (SCES2019)*, <https://journals.jps.jp/doi/pdf/10.7566/JPSCP.30.011174>.
- [56] A. A. Aligia, *J. Phys.: Condens. Matter* **24**, 015306 (2011).
- [57] A. A. Aligia, *Phys. Rev. B* **89**, 125405 (2014).
- [58] S. Hershfield, J. H. Davies, and J. W. Wilkins, *Phys. Rev. B* **46**, 7046 (1992).
- [59] Y. Meir and N. S. Wingreen, *Phys. Rev. Lett.* **68**, 2512 (1992).
- [60] A. C. Hewson, *J. Phys.: Condens. Matter* **13**, 10011 (2001).
- [61] G. Zaránd, L. Borda, J. von Delft, and N. Andrei, *Phys. Rev. Lett.* **93**, 107204 (2004).

- [62] S. Kehrein, Phys. Rev. Lett. **95**, 056602 (2005).
- [63] A. Oguri, Y. Teratani, K. Tsutsumi, and R. Sakano, Phys. Rev. B **105**, 115409 (2022).
- [64] A. C. Hewson, A. Oguri, and D. Meyer, Eur. Phys. J. B **40**, 177 (2004).
- [65] Y. Nishikawa, D. J. G. Crow, and A. C. Hewson, Phys. Rev. B **82**, 115123 (2010).
- [66] Y. Nishikawa, D. J. G. Crow, and A. C. Hewson, Phys. Rev. B **82**, 245109 (2010).
- [67] A. Oguri, R. Sakano, and T. Fujii, Phys. Rev. B **84**, 113301 (2011).
- [68] A. Oguri, Phys. Rev. B **85**, 155404 (2012).
- [69] K. Tsutsumi, Y. Teratani, R. Sakano, and A. Oguri, Phys. Rev. B **104**, 235147 (2021).
- [70] This limit of strong tunnel asymmetry $\gamma_{\text{dif}} \rightarrow \pm 1$ is meaningful for investigating asymptotic behavior of $C_V^{(3)}$ although it represents the situation where one of the leads is disconnected and the current is determined by Eq. (2.19).